A MECHANISM FOR SELECTION OF SCREW-TYPE DENTAL IMPLANTS FOR PATIENTS WITH LOW-DENSITY AND OSTEOPOROTIC BONE

RAM HARI KHATRI KC

MASTERS OF SCIENCE IN ENGINEERING PHYSICS- MECHANICAL ENGINEERING

UNIVERSITY OF CENTRAL OKLAHOMA

EDMOND, OKLAHOMA

MAY 2020

MASTER THESIS

SUBMITTED TO THE FACULTY OF THE GRADUATE COLLEGE OF UNIVERSITY OF CENTRAL OKLAHOMA

IN PARTIAL FULFILLMENT OF REQUIREMENTS OF DEGREE OF MASTER OF SCIENCE

MAY 2020

A MECHANISM FOR SELECTION OF SCREW-TYPE DENTAL IMPLANTS FOR PATIENTS WITH LOW DENSITY AND OSTEOPOROTIC BONE

Thesis Title

Ram Hari Khatri K C

Author's Name

05/04/2020

Date

Jackson College of Graduate Studies at the University of Central Oklahoma

A THESIS APPROVED FOR

PARTIAL FULFILLMENT OF REQUIREMENTS OF DEGREE OF MASTER OF SCIENCE

By

Abdellah Ait moussa — Digitally signed by Abdellah Ait moussa Date: 2020.05.05 16:40:55 -05'00'

Committee Chairperson

Mohammad Robiul Hossan — Digitally signed by Mohammad Robiul Hossan Date: 2020.05.05 22:24:43 -05'00'

Committee Member

Morshed Khandaker — Digitally signed by Morshed Khandaker DN: cn=Morshed Khandaker, o=University of Central Oklahoma, ou, email=mkhandaker@uco.edu, c=US Date: 2020.05.07 10:05:02 -05'00'

Committee Member

Committee Member

ACKNOWLEDGEMENT

I would like to express my sincere gratitude to the most amazing, talented, motivated and down-to-earth committee chair and supervisor, Dr. Abdullah Ait Moussa, who has the attitude to convince and encourage me even during the toughest situation and motivated me to stay focused. Without his guidance, persistent help and selflessness this thesis wouldn't have been completed.

I would also like to remember my committee members Dr. Morshed Khandaker and Dr. Mohammad Robiul Hossan for being there encouraging and supporting my research. I would like to acknowledge my friends Mr. Xainkun Zang and Mr. Desmond Sama with whom I shared the lab most of the time helping and encouraging each other during the difficult situation and tackling technical problems as a team.

I am indebted to my parents Mr. Shree Ram Khatri KC and Mrs ShyamKala KC, my wife Asmita Thapa, sister Laxmi Khatri KC and brother Keshav Khatri KC who believed in me and helped me in any way possible to encourage and keep me going. Without their constant inspiration this book would not have been possible.

I thank everyone who constantly supported me during the most difficult and panicking times and showed me the path to overcome such situations.

May god bless everyone!

ABSTRACT

Dental implants surgery are one of the most common and an all-time-high demand medical procedure with almost 450,000 dental implants being placed every year with a success rate of 95%. An ideal implant should be biocompatible, withstand compressive loadings and should possess long-life mechanical stability with the surrounding tissues. The initial stability of implant on cortical bone is very strong however life span of implants on trabecular bone is very high almost 95% compared to that of cortical bone.

Our goal in this research is to develop a standard for the selection of dental implants for the patients with low density and osteoporotic jaw bone. As a first step a gyroid model was developed which resembles the trabecular tissue. A basic gyroid model equation is supplied with a variable *b* which is simulated in Wolfram Mathematica to develop gyroids with different volume fraction. Changing the value of *b* from -1 to 1.35 gave us gyroid network which should be checked for mechanical response. To analyze the mechanical response under compression loading, the generated gyroid was imported into Solidworks then supplied with printing parameters in slicer software for the purpose of 3D printing. Trabecular bone tissue shows bilinear elastic-plastic and dual non-linear and ductile nature. So as a second objective of this research, composites like ABS, glass fiber and LLDPE were homogenously mixed which were bought in pallet form and then the filaments were extruded from the mixed composite. Our goal was to 3D print the gyroid with the filaments made from composite and perform compression test which would give us an acceptable range of modulus of elasticity. To determine the correct proportion of composites 10 samples each of 5%, 6%, 7.5%, 9%, 10%, 12%, 15% and 17% glassfiber reinforced ABS were 3D printed and tested for compression and the young's modulus of 10% and 12% GF ABS was found 1917 MPa and 2125 MPa respectively which is close to several literatures. Then 10 samples of gyroids were

printed with 12% GF ABS composition and the average modulus was found to be 1949 MPa with some corrective factor for the loss due to printing temperatures and printing conditions. Development of screw threaded implants couldn't be carried in this research because of limited time and tools and equipment. One important future task can be to find a way to extrude the filaments using LLDPE and 3D print the samples for test. Test samples using LLDPE can easily provide the bilinear elastic-plastic curve under compression test to verify the morphological as well as mechanical properties of trabecular bone.

LIST OF SYMBOLS

CAD	Computer Aided Design
FDM	Fused Deposition Modeling
FEA	Finite Element Analysis
TGB	Trabecular Gyroid Bone
OP	Osteoporotic
RVE	Representative Volume Element
Tb.Sp	Trabecular Spacing/ Separation
Tb.Th	Trabecular Thickness
V_f	Volume Fraction
SMI	Structural Model Index
BS	Bone Surface Area
$S^{'}$	Change of Surface Area
BV	Bone Volume
TV	Total Volume
E_{pre}	Pre-elastic Modulus
E_{post}	Post-elastic Modulus
σ_y	Compressive yield Strength

E_{app}	Apparent Young's Modulus
ρ_{app}	Apparent Density
STL	Stereolithographic
API	Application Programming Interface
3D	Three-Dimensional
AM	Additive Manufacturing
ABS	Acrylonitrile Butadiene Styrene
PLA	Polylactic Acid
PETG	Polyethylene Terephthalate Glycol
GF	Glass Fiber
LLDPE	Linear Low Density Polyethylene
LDPE	Low Density Polyethylene
HDPE	High Density Polyethylene
ASTM	American Society for Testing and Materials

TABLE OF CONTENTS

LIST OF FIGURES

LIST OF TABLES

CHAPTER 1

INTRODUCTION

1.1. Overview

Dental implants are considered to be one of the successful and effective medical choice which has been commonly used for the replacement of delicate teeth or to restore missing teeth caused due to old age, accidents and even for esthetic purpose. (Mathieu, et al., 2014) Till date there is not any best dental implant techniques however several clinical advancement has helped in achieving successful treatment even in few weeks to some months. Osseointegrated dental implants are one of many such advancement which allows a patient to enjoy a permanent and healthy teeth. It is a direct structural and functional connection of living bone and load carrying endosseous implant at light microscopic level. (Davies, 2003)

According to a research done in 2014 by American Association of Oral and Maxillofacial Surgeons, 69% of adults ages 35 to 44, in USA, have lost at least one permanent tooth due to an accident, gum disease, failed root canal or tooth decay. Further, 26% of adults have lost all of their permanent teeth by age 76. As a result, 100,000-300,000 dental implants are placed each year which is almost equal to the number of artificial hip and knee joints placed per year. (Gaviria L. , Salcido, Guda, & Ong, 2014) Today, over 30 million people do not have teeth in one or both jaws and more than 15 million people have crowns or bridges. Approximately 450,000 osseointegrated dental implants are being placed every year, with almost 95% success rate. (Agarwal, 2018)

1.1.1. Anatomy

Human bone are microscopically classified into four different hierarchies. (Doland, Dwight, & Tony, 2006)

i) mineralized collagen fibrils (approximately 0.1 micron),

ii) lamellar and woven bones (approximately 10 microns),

iii) primary lamellar and laminar bones (approximately 500 microns)

iv) trabecular and cortical bones (greater than 1000 microns)

The bone quality is categorized into four different classes based on the relative proportion of cortical bone to trabecular bone. (Zohdi & Wriggers, 2008) Class I bone has the majority of cortical bone. It is sometimes called compact bone which is the densest bone in human skeleton. The porosity of the cortical bone is usually below 30 %, that being said, the volume fraction of cortical bone is above 70%. (Muller, et al., 1998) (Doland, Dwight, & Tony, 2006) Similarly Class IV bone primarily consists of trabecular bone and is also known as spongy bone or cancellous bone. It is the least dense bone with a porosity above 40%, that being said, the volume fraction of trabecular bone is below 60%. Trabecular bone in its early age is relatively dense and is observed to be plate-like while in osteoporotic person it tends to become slender and rod like as a result of decrease in bone density. (Muller, et al., 1998) Trabecular bones are the interconnected network of rods and plates of thickness 100 to 300 microns and inter-trabecular spacing of 500 to 1500 microns. (Doland, Dwight, & Tony, 2006) The density of the compact bone is in the range of 1800-2000 kg/m^3 while that of a trabeculae is 1820 kg/m^3. (Gibson & Ashby, 1999)

While performing dental treatments, the implants are placed into the mandible and maxillary bones, which consists of a dense layer of cortical bone surrounding a lesser dense trabecular bone. A detail anatomy of human jaw bone is shown in figure 1 below.

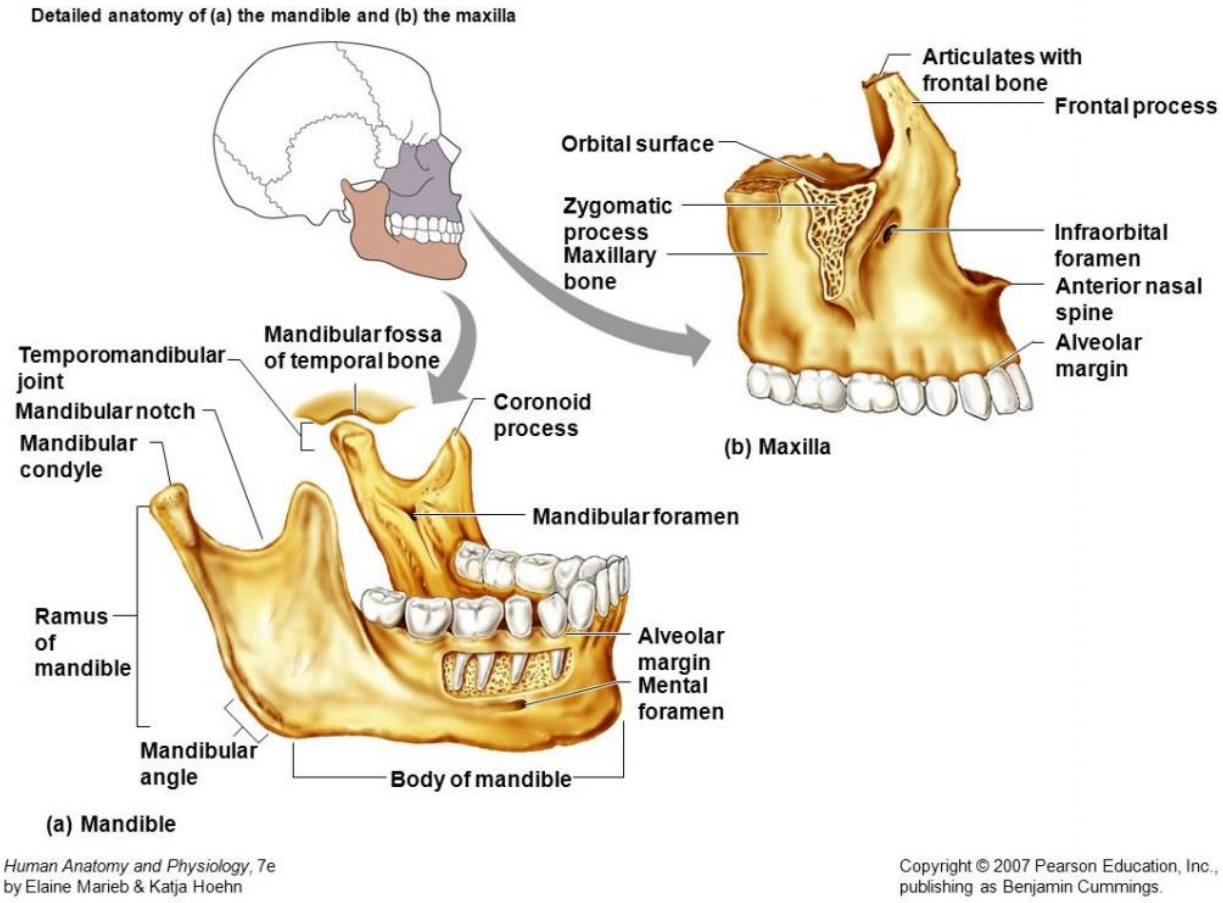

Figure 1: (a) Mandible (b) Maxilla of Human Jaw Constituting Trabecular Bone and Cortical Bone

1.1.2. Implant Design

There are several factors that needs to be considered for the successful dental implantation. The biocompatibility of the implant, which is both the compatibility of material with the tissue and also the ability to perform the desired function, is the most important factor to be considered. For improving osseointegration for a long term success of the implant we also need to consider the design of dental implant, biomechanical factors, surface characteristics, oral health of patient, bone quality and the treatment techniques. (Gaviria L. , Salcido, Guda, & Ong, 2014)

Several biomaterials used for manufacturing dental implants are metals, ceramics, polymers, carbons and the combinations of these. Pure titanium and titanium alloys like Ti-6Al-4V are the most commonly used implant materials. Since polymers are softer and flexible, they are prone to low mechanical strength. Bio ceramics like hydroxyapatite also have low strength but have excellent biocompatibility. Metals like zirconium, gold and titanium alloys shows greater strength but has poor bone to implant contact. As pure titanium is a light metal with exceptional biocompatibility, high stiffness and high resistance to corrosion, it is still considered as number one choice when it comes to dental implants. (Gaviria L. , Salcido, Guda, & Ong, 2014)

Implants are classified based on their geometry, shape, surface, function and materials. All implants are widely divided into an osseous portion, a transmucal component and the restoration which consists of crown, bridge abutment or anchors. (Drysdale, et al., 2012) A general categorization of the dental implants are shown in Fig 2.

Figure 2: Dental Implants Parts (1) Crown, (2) Screw, (3) Abutment (4) Fixture

The implants are designed as such it helps in achieving mechanical stability and also promotes strong bone-implant interaction over time through osseointegration. Threaded cylindrical or root-form implants are the most popular category of dental implant because of great initial retention strength. Thread parameters like thread pitch, thread height and configuration (v-shaped, square-shaped etc.) also play vital role. Pitch predominantly plays a role in allocating surface area for bone interaction. Lesser the pitch, the lesser will be the maximum effective stress as a result, less stress exposed to bone is required to hold the implant stable. (Gaviria L. , Salcido, Guda, & Ong, 2014). Similarly, truncated v-thread (0.1 mm width thread apex) and a large square thread (0.36 mm thread width) helps in distributing the stresses evenly throughout the implant while some studies suggests the thread profile has no role in stress distributions. (Geng, Ma, Xu, Tan, & Liu, 2004) Kim et al. compared threaded cylindrical implants with threaded conical implants and found that the initial stability of conical implants is greater than cylindrical implants, however, cylindrical implants had higher success rates than the other. Conical implants causes over compression on the surrounding bone matrix. (Kim, Baek, Kim, & Chang, 2008) Modern dental implants have a rough surface to increase the area of bone-implant contact while some implant surfaces are coated with bioactive substances such as fluoride to encourage osseointegration. (Drysdale, et al., 2012)

1.1.3. Bone Regeneration- Biological Process

Formation and growth of the bones around the implant can be broadly described in two biological processes- distance osteogenesis and contact osteogenesis. Both distance and contact osteogenesis occurs in every endosseous healing site but their biological significance depends on the differences in structure and composition of the bone/ implant interface. (Davies, 2003) In distance osteogenesis, new bone is formed on the surface of the old bone in the peri-implant site. The existing bone provides the required osteogenic cells, which are generated usually during the blood

clot to the surface of the implant. Here the new bone is not forming on the implant but is surrounded by the cells to approximate the implant surface. (Maria, Helena, & Joao, 2011) Similarly, in contact osteogenesis, new bone begins to form on the surface of the implant and grows in opposition to the implant surface. Initially, no bone is present on the surface of the implant; the implant surface has to be colonized by bone cells before bone matrix formation starts. In Class III and Class IV bones, contact osteogenesis can be optimized by implant surface design to ensure early implant stability. (Davies, 2003)

In both distance and contact osteogenesis, the bone formation occurs in three phases: osteoconduction, de novo bone formation and bone remodeling. (Davies, 2003) When the space between the existing bone and the implant is filled with the blood clots during the preparation of the implant site there is the recruitment of the osteogenic cells and they migrate to the implant surface. This early stage of bone formation where the osteogenic cells position themselves on the surface of the implant to make the bone matrix is known as osteoconduciton. Now the osteogenic cells which reaches the implant surface needs mineralization for the formation of bone. In this process of *de novo* bone formation, the collagen-free organic matrix is differentiated from the initiation of collagen fiber. (Davies, 2003) Finally, the matrix secreted by the osteoblast cells mineralizes into new bone formation. After the completion of these two initial bone formation process, the remodeling phase takes place.

1.1.4. Bone Regeneration- Mechanical Factors

Several mechanical factors plays vital role for a successful implant stability. The quality of the implant surface and the mechanical quality of the bone tissue around the bone-implant interface determines the nature of the remodeling. (Lin, Li, Li, & Swan, 2009) When a surgery is performed, the interfacial bone undergoes remodeling by substituting with mature lamellar bone, but when the

bone and the implants are not in immediate contact, rapid woven bone filling occurs which is weak in nature and even a small micro movements prevents healing forming a fibrous tissue. (Heller & Heller, 1996) Pilliar et al., 1986 suggests that a micromotion between the implant and bone tissue should not exceed 150 micro-meter. But some studies has shown that a relatively small micro movement accelerates the bone remodeling phase but the threshold of it is yet to be determined. (Pilliar, Lee, & Maniatoloulos) In general, we can say that some smaller occlusal load on the implant, stimulates early healing stages through osteoconduction of cells through blood clot, while maintaining moderate levels of micro motions within the implant-bone interface. (Lin, Li, Li, & Swan, 2009)

A balance between the initial stress and a good primary stability is the key factor for the long term success of the implant stability. The cortical bone-implant interface is the most important region regarding the success because of highest bone stress occurring in cortical bone around the neck. (Sutpideler, Eckert, Zobitz, & An, 2004) Bone formation is accelerated when a force or displacement controlled mechanical loading is applied at low frequency (<10 Hz). A higher frequency (>10 Hz) can also lead in improved bone formation in the peri-implant surroundings but the stress generated should also be taken care of. (Ogawa, et al., 2011)

1.1.5. Trabecular Bone for Dental Implants

Cortical bone are dense and compact and hence can withstand larger torsional loading while trabecular bone are porous and can withstand greater compressive loadings. Healing can occur in both cortical and trabecular regions, however, the formation of the osteogenic cells, which are the key agents in bone healing are found in abundance in trabecular regions as such cancellous bone has a very high surface area. So the remodeling process is far quicker in trabecular bone than in cortical bone. (Davies, 2003) The initial stability of the implant on cortical bone is surprisingly

strong because of the dense nature of the bone which can strongly hold the implants. However, studies have proven that the life span of implants on trabecular bone is higher (around 95% success rate) because of more availability of the osteogenic cells which are produced in the bone marrow. As a result cancellous bone is remodeled more often than the cortical bone. (Rho, Kuhn-Spearing, & Zioupos, 1998)

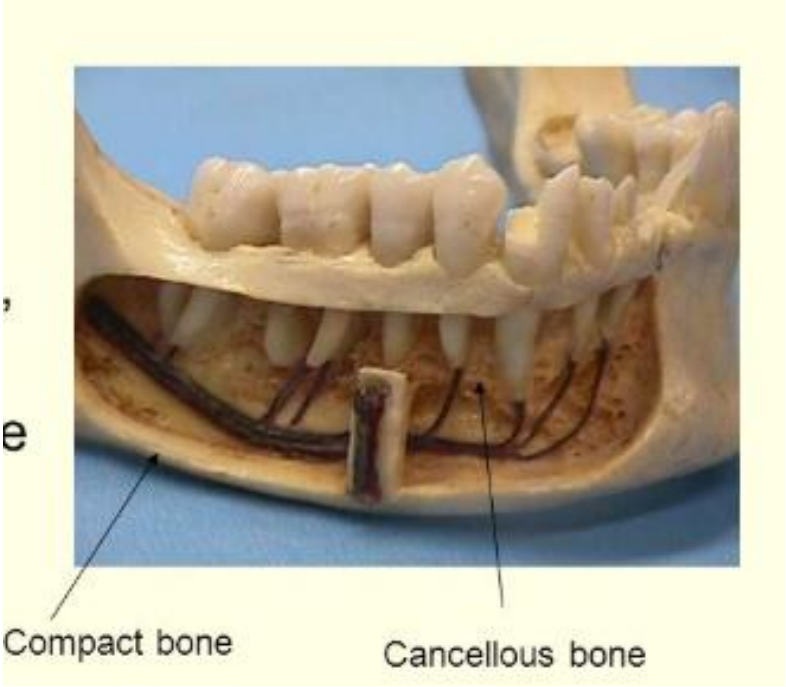

Figure 3: Compact and Concellous bone in human jaw

A study done by Hart. et. al. as illustrated in figure 4, on the bone tissue found that the cortical bone is more stiff and has a high resistance to stress and low resistance to strain (2% yield) while trabecular bone showed low resistance to stress and high resistance to strain (50% yield). (Hart, et al., 2017). This must be because of the porous nature of trabecular bone tissue. (Hart, et al., 2017)

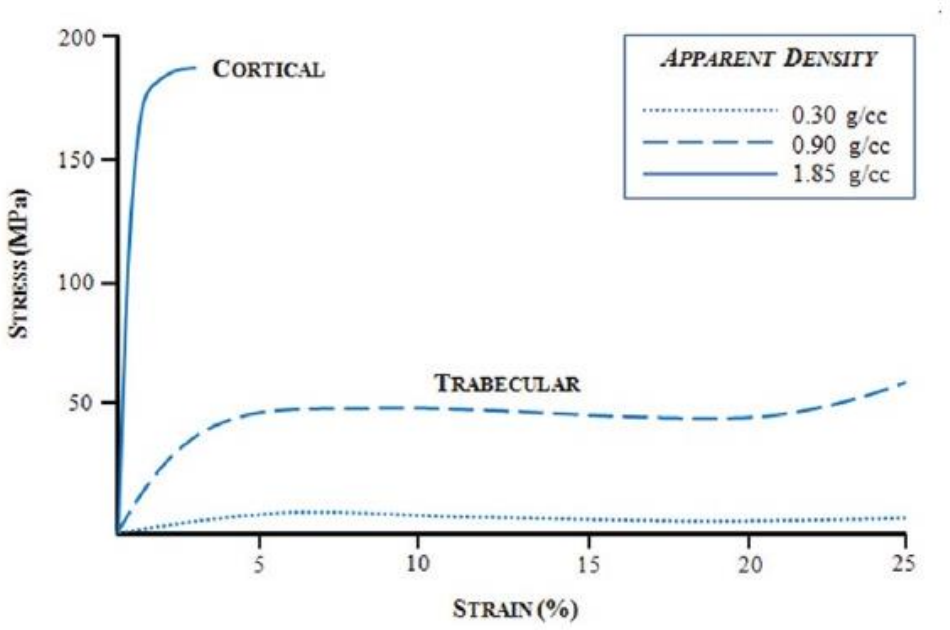

Figure 4: Stress-strain characteristics of cortical and trabecular bone tissue

1.2 Research Objectives

1.2.1. Specific Aims

Today dental industry has marketed wide selections of dental implants. But still no recommendation or standardization exists among the scientists with regard to the best practices for selecting a patient specific dental implants. As discussed earlier, several studies have emphasized the importance of implant-bone contact area, implant surface morphology, roughness and treatment to the success of the primary & secondary stability of dental implants. The choice of implant geometry, including but not limited to the size, thread profile, pitch and surface should ensure the appropriate distribution of the biomechanical forces during loading and unloading (i.e. chewing) to maintain a balance between bone remodeling resorption and appositional ingrowth during tertiary phase, especially for patients with low density and osteoporotic bone.

Our long-term goal is the development of a standard for the selection of endosseous dental implants for patients with low density and osteoporotic jaw bone. Towards achieving this goal, the overall objective of this application is the development of an efficient mechanism that can realistically and accurately differentiate between favorable and adverse geometrical features within screw-type dental implants to the maintenance of osseointegration in patients with low density and osteoporotic bone. Our central hypothesis is that maintenance of osseointegration during the tertiary phase of dental implantation in patients with low density and osteoporotic jaw bone is contingent on select features within the implant geometry; inadequate choice can be detrimental to the sustainability of the implant-bone natural fixation.

To test our central hypothesis in a consistent and non-invasive manner, specific aim.1 with subtasks 1, 2 &3 and specific aim.2 with subtasks 1&2 were laid out.

- *Specific Aim.1-Subtask.1:*

  Develop and benchmark a versatile and realistic Computer Aided Design (CAD) model of the trabecular bone that is morphologically and mechanically accurate for representing low-density and osteoporotic jaw bone.

- *Specific Aim.1-Subtask.2:*

  Synthesize a filament composite for Fused Deposition Modeling (FDM) (i.e. 3D printing) of a trabecular jaw bone that is morphologically and mechanically accurate for representing low-density and osteoporotic jaw bone.

- *Specific Aim.1-Subtask.3:*

  Develop a versatile and realistic CAD model of a screw-type implant that bears the majority of geometrical features in commercially available dental implants.

- *Specific Aim.2-Subtask.1:*

  Use Finite Element Analysis (FEA) and optimization to identify key geometrical features within the implant design that favor uniform transfer of occlusal load between implant and patient-specific trabecular bone.

At the successful completion of this project, expected outcomes include (1) the development of a novel trabecular jaw bone analogue that can adapt to patient-specific bone morphology, be easily synthesized, and accurately reproduce the mechanical behavior of real trabecular bone upon compression. (2) The development of a versatile and realistic CAD model of a dental implant with key geometrical features that contribute to the long-term maintenance of osseointegration. Results will have a positive impact on the development of synthetic bone analogues, and the advancement of dental biomechanics, more importantly the appropriate selection of screw-type dental implants that improve the durability of the natural fixation and enhance the retention of trabecular bone tissue in patients with low-density and osteoporotic bone.

1.2.2 Importance of the Problem

Low density and osteoporotic bone have the lowest dental implantation success rate around 65%. (Lin, Li, Li, & Swan, 2009) Generally, survival rates have been recorded as high as 90% after 15 years. (Drysdale, et al., 2012) The formation and stability of new bone around a dental implant is a combination of resorption and bone apposition, and a balance must be maintained between these processes to ensure the long-term survival of the implant natural fixation. The sustained maintenance of this fixation is contingent on the biomechanical stimulus within the bone-implant construct. Inadequate transfer of occlusal load can cause stress shielding and stress overload over the implant-bone interface, hence inhibiting bone remodeling formation within the osseointegrated

layer. This effect is more pronounced in low density and osteoporotic bone which explains their lower success rates.

1.2.3. How the Proposed Project will Advance the Fields of Dentistry and Orthopedics

Evolving implant designs together with improvements in surgical procedures and individualized treatments have grown the field of dental implantology, and we now see almost a million dental implant procedures conducted annually, worldwide. (Davies, 2003) The current study will sustain this growth by facilitating a dental implant design process to accommodate patient-specific trabecular bone quality and quantity, and particularly, improve the success rate of dental implantation in patients with low-density and osteoporotic bone. Furthermore, the high rate of periprosthetic fracture associated with the use of uncemented stems in patients with osteoporosis, raised many concerns about the stem type used in the weakened proximal region of the hip. Successful implant designs require careful manipulation of the implant geometry and material (Aitmoussa, Yadav, Fisher, & Khandaker, 2017) together with realistic testing on substrates that can accurately serve a patient-specific bone. (Aaitmoussa & Yadav, 2017) The proposed Trabecular Gyroid Bone (TGB) model can facilitate this task and help produce better designs.

1.2.4. Innovative Approach to be Developed or Used

Conventional methods for testing implants rely on cadaver specimens. Cadaver bones are suboptimal for myriad reasons, including issues of cost, availability, preservation, and inconsistency among specimens. (Dunlop, Chong, Lucas, & Cook, 2008) (Szivek & Gealer, 1991) Further, currently available synthetic bone analogues disproportionately represent a patient-specific bone quality and quantity (Elfar & Stanbury, 2014) and hence are unable to provide neither conclusive nor reliable test results. The current application aims at overcoming these drawbacks by providing accurate and reproducible testing substrates that are based on a patient-specific bone

quality and quantity. Further, it allows the identification of key geometrical features that can ensure sustainability and maintenance of the implant natural fixation in patients with low-density and osteoporotic bone.

1.3. Organization of Thesis

Chapter 1

This chapter basically gives the scenario of osteoporosis jaw bone and the need assessment of this thesis. The anatomy of jaw bone, cause and present cases of people with osteoporosis and the bone regeneration process are briefly described. The reason behind focusing on the trabecular bone rather than the cortical bone is also summarized in this chapter and it finally describes our aims, goals and objectives of this thesis.

Chapter 2

Chapter two focuses on development of trabecular bone tissue model. Gyroid networks are created doing some numerical analysis to best resemble the trabecular nature of the bone and it describes the morphological parameters like volume fraction, trabecular spacing, trabecular thickness and structural model index. In the later part, CAD model of the gyroid network is developed which can be imported in the slicer software for the purpose of 3D printing.

Chapter 3

This chapter basically deals with the development of the screw threaded implant. Most of the theoretical part and literature reviews are covered in chapter one also. It describes the basic mathematical equation used for developing the thread profile and other parametric profiles however, fabrication and experimental parts couldn't be included because of limited time and complex fabrication techniques.

Chapter 4

This chapter describes everything about 3D printing, composite materials, materials used for 3D printing, procedures, techniques, 3D printer troubleshooting, variable selection in slicer software. The methods of printing test samples and actual gyroids and the compromise made to print the gyroid networks resembling the trabecular nature of jaw bone is described in this chapter. Similarly, the test mechanical test procedures, experimental results, reason of deviation of the test results and comparison of data with several composition of pure ABS and GF ABS are tabulated in this chapter.

Chapter 5

This last chapter of this thesis gives the conclusion and future work.

CHAPTER 2

DEVELOPMENT OF A VERSATILE MODEL OF THE TRABECULAR BONE

2.1 Abstract

In this chapter, we propose a model for the trabecular bone based on the gyroid. A gyroid network resembles the relevant mechanical properties of trabecular bone. Human trabecular bone possess several range of volume fraction (V_f) meaning the bone is not compact everywhere and has varying bone density.

A basic mathematical equation

$$\cos(\omega x)\sin(\omega y) + \cos(\omega y)\sin(\omega z) + \cos(\omega z)\sin(\omega x) \geq b$$

is used to depelop a gyroid model. A solid surface resembling gyroid is developed using Mathematica Software (Wolfram Inc) by keeping the value of ω constant to 1 and only changing the value of control parameter b from 0.1 to 1.4. It is found that for a value of b greater than 1.3 the struts in the gyroid network begins to break and are no more connected to each other while for a value of b less than 0.1 it gave us compact bone structures. Note that, as the value of b increased from 0.1 to 1.4 the volume fraction of the unit cell decreased meaning the amount of bone in that cell decreased significantly. Likewise, trabecular thickness also decreased with the increase in the value of control parameter b however, the trabecular spacing possessed an increased quadratic relation with the increase in value of b. Those gyroid networks are imported in SolidWORKS in STL format and the CAD geometry is edited in QIDI slicer software to add the 3D printing properties.

2.2. Introduction

Trabecular bone is a complex material and is remarkable for its vast structural heterogeneity depending on its location and the age and physical health of the subject. In young or early age subjects, trabecular bones are dense and are arranged in a plate-like form while in elderly subjects, these bones are more porous and are usually arranged in rod-like form. Generally speaking, trabecular bone is a network of both plate-like and rod-like form representing variable porous structure. (Abhishek, 2014) In a morphological point of view, cortical bone contains void which are always smaller than 200 microns while that of trabecular bone is between 500 to 1500 microns. Its elastic and strength properties depend primarily on its apparent density, which typically lies between 1.8g/cm^3 and 2g/cm^3. (Carter & Hayes, 1977) High density polyurethane foams were generally perceived as suitable models for representing the elastic behavior of natural bone under compression. (American Society for Testing and Materials, 2009) However, none of the low-density polyurethane foams are universally accepted as models for osteoporotic (OP) or low density bone. (Patel, Shepherd, & Hukins, 2008) Over the years, a number of geometrical models were developed in an attempt to reproduce the micro/macroscopic structure and mechanical behavior of the trabecular bone under the various modes of loading and finite element (FE) setting. A novel model for trabecular bone based on minimal surface family of solids, called the gyroid, and has attracted more interest among scientists because of its similar morphological properties and mechanical behavior to real trabecular bone.

In this research, we will develop a gyroid network to produce a realistic CAD model of trabecular bone, as it is easy to construct, that resembles the morphology and mechanical behavior of a patient-specific real trabecular bone under compression. Such gyroid cells can be used to obtain properties of large scale bone.

2.3. Materials and Methods

2.3.1. Development and Morphological Analysis of the Gyroid Model

In this section, we describe the technique used to develop a versatile model of the mandibular trabecular bone, and the methods used to estimate and control the morphometric parameters of this model within a typical Representative Volume Element (RVE) that serves the general structure of the human trabecular bone.

2.3.2 Development of Gyroid Network

A minimal surface solid is the gyroid which has mean curvature of zero at every point. It is an infinitely connected periodic minimal surface containing no straight lines. It was first discovered by NASA scientist *Alan Schoen* in 1970 and since then it has been widely used in representing the cells preserving their morphological and mechanical properties. The basic mathematical equation of the gyroid model is described in equation 2-1

$$\cos(\omega x)\sin(\omega y) + \cos(\omega y)\sin(\omega z) + \cos(\omega z)\sin(\omega x) \geq b \qquad \text{(Eqn. 2-1)}$$

Where (x, y, z) are the Cartesian coordinates of a test point, (ω) is a number used to control the number of gyroid cells per unit volume. Changing ω changes the volume fraction of the unit cell and therefore the porosity and properties of the unit cell. This flexibility helps to model the densities of patient's bone more accurately. However, we have assumed $\omega = 1$ throughout as it yields a useful surface that is easily modeled in SolidWorks. Factor (b), on the other hand, may be dependent of the position and controls the general morphology of the resulting gyroid network. By varying the value of b we can modify the amount of bone in unit cell, i.e. deceasing the value of b increases the amount of bone and therefore increasing the volume fraction V_f and vice versa.

Equation 2-1, represents a family of two parameter minimal solid surface that are three fold periodic along the x, y, and z directions. The solid bounded by a network of these units will be used to describe the complex structure of the mandibular trabecular bone. To demonstrate the suitability of the gyroid model in equation 2-1 to serve this purpose, we produce a network of these units within a representative volume unit (RVE), then analyze the relation between several values of the control factor (b) and a number of known morphological parameters used in high-resolution micro-computed tomography (micro-CT) of the human trabecular bone, including the trabecular spacing (Tb.Sp), the trabecular thickness (Tb.Th), the volume fraction (V_f) and the structural model index (SMI).

The size of RVE must be small enough to represent the complex microscopic structure of the trabecular bone but large enough to manifest the propagation of a typical micro-mechanical fluctuation of the stress or strain between the constituent trabeculae. (Hill, 1952) As the mean trabecular thickness is approximately $100\mu m$, 2mm is sufficiently large for the RVE size. (Muller, et al., 1998) Hence we selected a cubic volume element size of 2×2×2 mm^3.

A self-developed computer program using the Mathematica Software (Wolfram.Inc) was used to map the solid surface satisfying the inequality in equation 2-1, for a number of values of the control factor (b), while keeping the parameter ($\omega = 1$). The program starts by creating a boundary mesh that accurately approximate the implicit surface of the gyroid network defined by equation 2-1. The unit vectors normal to each boundary mesh cell were calculated from the cross-product of two vectors joining different nodes within the cell. The total area of the sample (BS) was calculated by adding the surface areas of the respective boundary cells. The rate of change of the surface area (S') was also calculated following an infinitesimal normal displacement (Δr) of the surface mesh vertices of each cell in the outward direction ($S' = \Delta S/\Delta r$). The volume of the sample (BV) was

calculated from the surface integral of the dot product of the boundary cell surface area and its outward pointing normal using Gauss's theorem in equation 2-2. The parameters just calculated where used along within equation 2-3 to 2-6 to estimate the volume fraction, trabecular thickness, trabecular spacing and structural model index of the gyroid network within the RVE as well as their respective correlations with the control parameter *b* in equation 2-1.

$$d\vec{S} = \iiint div(\vec{n})\, dV \qquad \text{(Eqn. 2-2)}$$

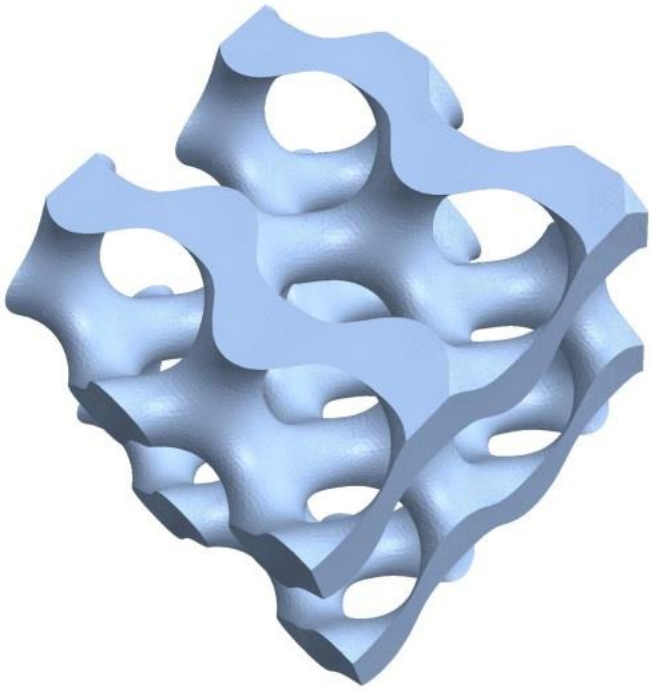

Figure 5: Representative volume Element of gyroid network (ω =1, b=0.75)

2.3.3. Morphometric Analysis of the Gyroid Network

2.3.3.1. Correlation with Volume Fraction

Volume fraction is defined as the ratio of the bone volume (BV) to the total volume (TV) of the bounding box for a unit gyroid. It is used to indicate the percentage of the bone volume within the

RVE. Larger values indicate a dense trabecular bone, while smaller values suggests a more porous trabecular structure.

$$V_f = \frac{BV}{TV} \qquad \text{(Eqn. 2-3)}$$

Where BV is the volume of the bone and TV is the total volume of the bone.

The volume fractions calculated for different values of the parameter (*b*) using the methodology of section 2.3.2 were plotted in the diagram in figure 6. Regression analysis indicated a direct linear relation between the volume fraction of the gyroid network within RVE and control factor *b* in equation 2-1. Furthermore, the span of the volume, suggests that the mathematical model of gyroid can potentially be used for a wide range of trabecular bone structure including low density and in some extreme cases, osteoporotic trabecular bones where the volume fractions can reach levels as low as 5%. However, at the V_f around and below 5%, there is a chance of obtaining disconnected struts, while at very high values around 60% the cell walls fuse together forming closed cells.

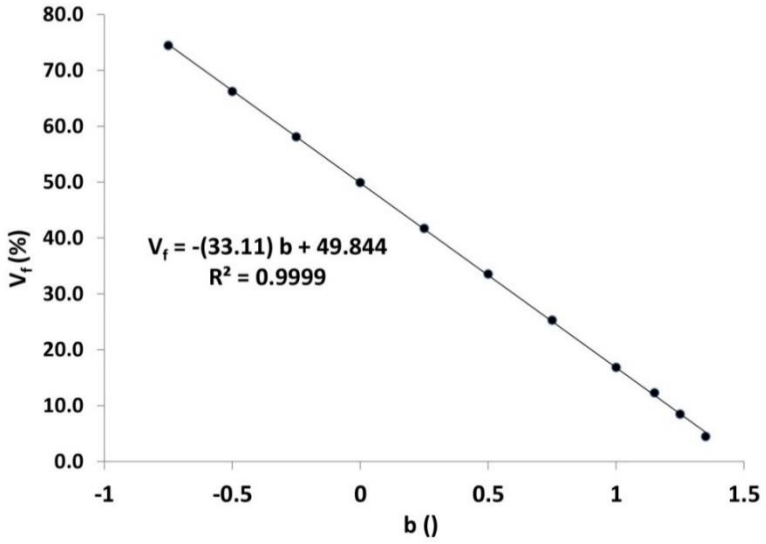

Figure 6: Volume Fraction (V_f) vs Control Parameter (b)

2.3.3.2. Correlation with Trabecular Thickness

Trabecular thickness (Tb.Th) is the mean thickness of the trabeculae which usually lies in the range of 200 and 400 μm depending on the bone function and location in the body. (Jung, et al., 2013) The average trabecular thickness (Tb.Th) of the gyroid network structure was estimated for rod-like structures using equation. 2-4. (Day, et al., 2000)

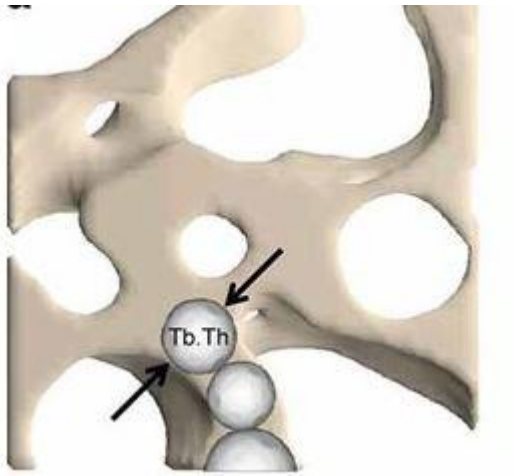

Figure 7: Trabecular Thickness in a Gyroid Strut

Source: (Bouxsein, et al., 2010)

Regression analysis of the calculated data in the chart of figure 8 indicate a direct linear relation between the trabecular thickness of the gyroid network and the control parameter *b* in Eqn. 2-1.

$$\text{Tb. Th} = \frac{4}{\frac{BS}{BV}} \qquad \text{(Eqn. 2-4)}$$

Where BS is the total surface area of the bone and BV is the volume of bone.

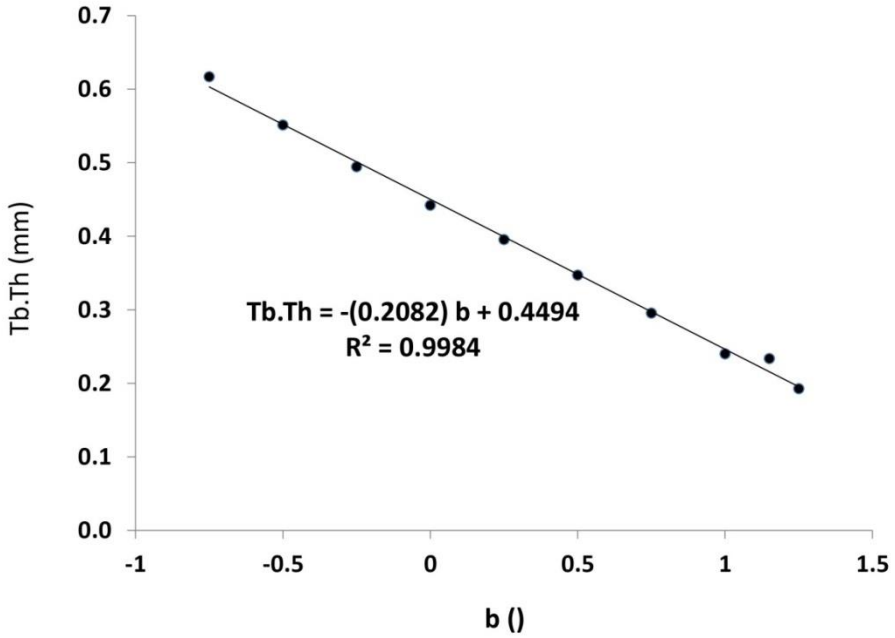

Figure 8: Trabecular Thickness (Tb.Th) VS Control Parameter (b)

2.3.3.3. Trabecular Separation/ Spacing (Tb.Sp)

The average trabecular separation (Tb.Sp) of the gyroid network structure is a measure of the average thickness between trabeculae. Trabecular spacing for a rod like structure was calculated using equation 2-5. (Day, et al., 2000)

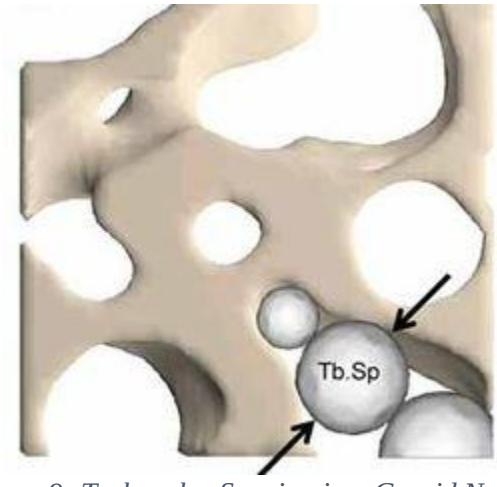

Figure 9: Trabeuclar Spacing in a Gyroid Network

Source: (Bouxsein, et al., 2010)

Regression analysis of the data as depicted in figure 10 indicate a direct quadratic relation between Tb.Sp with the control parameter *b* in equation 2-1.

$$\mathrm{Tb.Sp} = \mathrm{Tb.Th}\left(\sqrt{\frac{\pi}{4}\left(\frac{TV}{BV}\right)} - 1\right) \qquad \text{(Eqn. 2-5)}$$

Where TV is the total volume of bone and BV is the volume of bone.

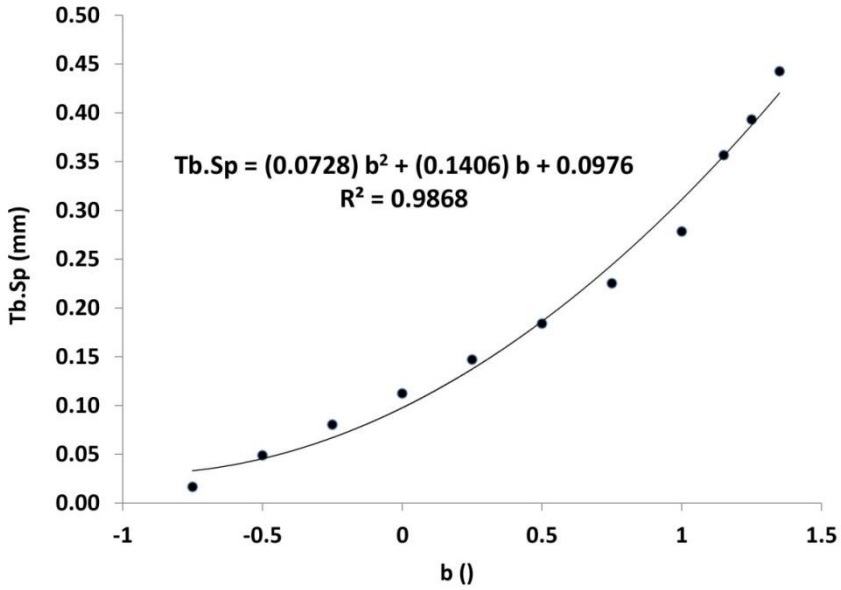

Figure 10: Trabecular Spacing (Tb.Sp) VS Control Parameter (b)

2.3.3.4. Structural Model Index

Structural Model Index (SMI) is a method intended for determining the plate-like or rod-like geometry of trabecular structures. It provides a measure of the aspect ratio of the trabeculae within the gyroid structure. It uses the change in surface area as volume increases infinitesimally to calculate SMI=0 for plates, 3 for rods and 4 for solid spheres. (Hildebrand & Ruegsegger, 1997) An important assumption underlying SMI is that the entire bone surface is convex and therefore we have a positive SMI. However SMI is negative in the case of concave surfaces, which are

common in trabecular bone so it might not be a good idea to quantify real bone structures. (Phil, Ohlsson, & Michael, 2015)

The SMI of the gyroid network within the RVE was calculated using equation 2-6 (Hildebrand & Ruegsegger, 1997) and according to the diagram in figure 11, the SMI of the gyroid network model within the RVE is in direct linear relation with the control parameter *b* in Eqn. 2-1.

$$\mathrm{SMI} = \frac{6[BV\ (dS/dr)]}{BS^2} \qquad \text{(Eqn. 2-6)}$$

Where BV denotes the volume of the bone material in the structure, BS is the total surface area of bone and dS/dr is the change of surface area S with the half thickness, r.

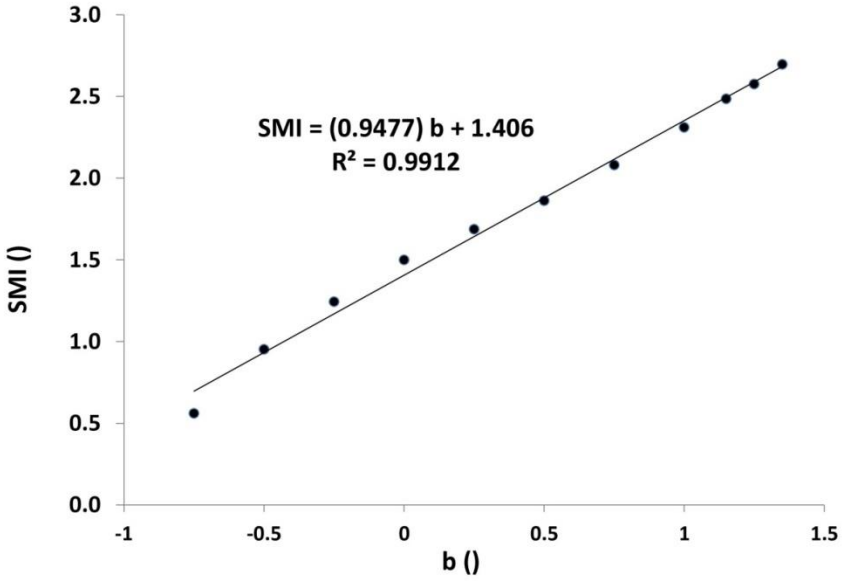

Figure 11: Structural Model Index (SMI) VS Control Parameter (b)

2.3.4 Summary of the Morphometric Study

The results of the morphometric analysis using the representative volume element of the gyroid network revealed the close relation between the control parameter (b) in equation 2-1 and the morphometric parameters used in the description of the human trabecular bone. The correlation was nearly linear for the volume fraction, structure model index and the trabecular thickness while nearly quadratic for the trabecular spacing. Furthermore, by changing the values of the control parameters between ($-1 \leq b \leq 1.35$), we can achieve morphometric values that fall within the range of human trabecular bone. (Keller, 1994), (Stauber & Muller, 2006)

Unfortunately, the analysis up to this point is incomplete since the use of the gyroid network may not guarantee similar mechanical response to static or dynamic loads unless; appropriate material properties and material behavior are satisfied. To that end, we analyze the mechanical response under compression load to serve this purpose.

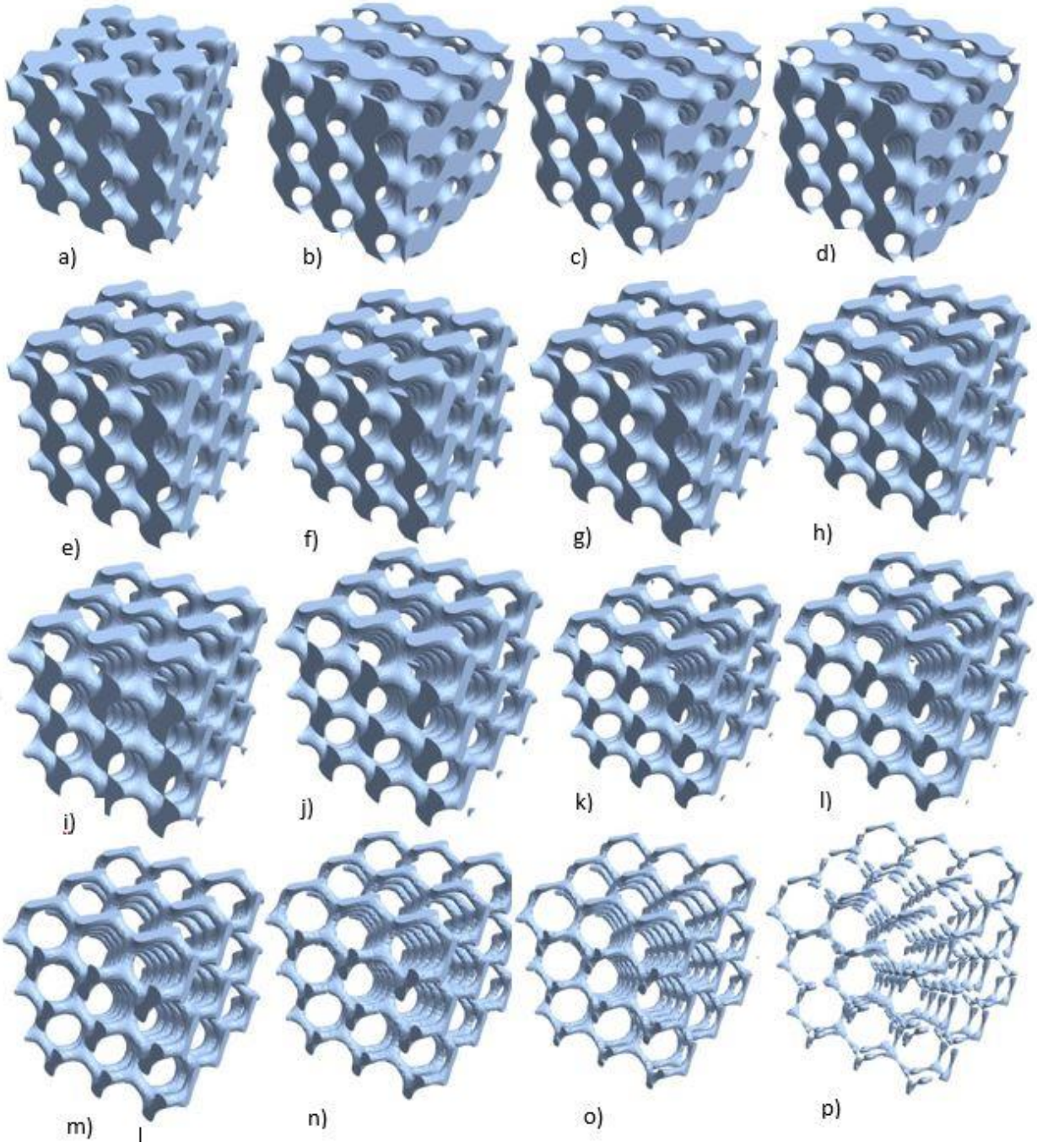

Figure 12: Gyroids developed using Wolfram Mathematica taking w=1 and and value of b as a) b=0.0, b) b=0.1, c) b=0.2, d) b=0.3, e) b=0.4, f) b=0.5, g) b=0.6, h) b=0.7 i) b=0.75, j) b=0.8, k) b=0.9 l) b=1.0, m) b=1.1, n) b=1.2 o) b=1.3 p) b=1.4

2.4. Determination of the Mechanical Properties of the Gyroid Network

The mechanical response of the gyroid network to an applied static or dynamic load depends not only on the morphology of the gyroid structure within the RVE, but also, on the mechanical properties and behavior of the material of the gyroid unit. Bayraktar, H.H et al. 2004 confirmed the dual non-linear and ductile nature of the trabecular bone tissue and a bilinear elastic-plastic strain hardening material behavior such as that in figure 13 was used to approximate the general non-linear behavior. (Bayraktar, et al., 2004)

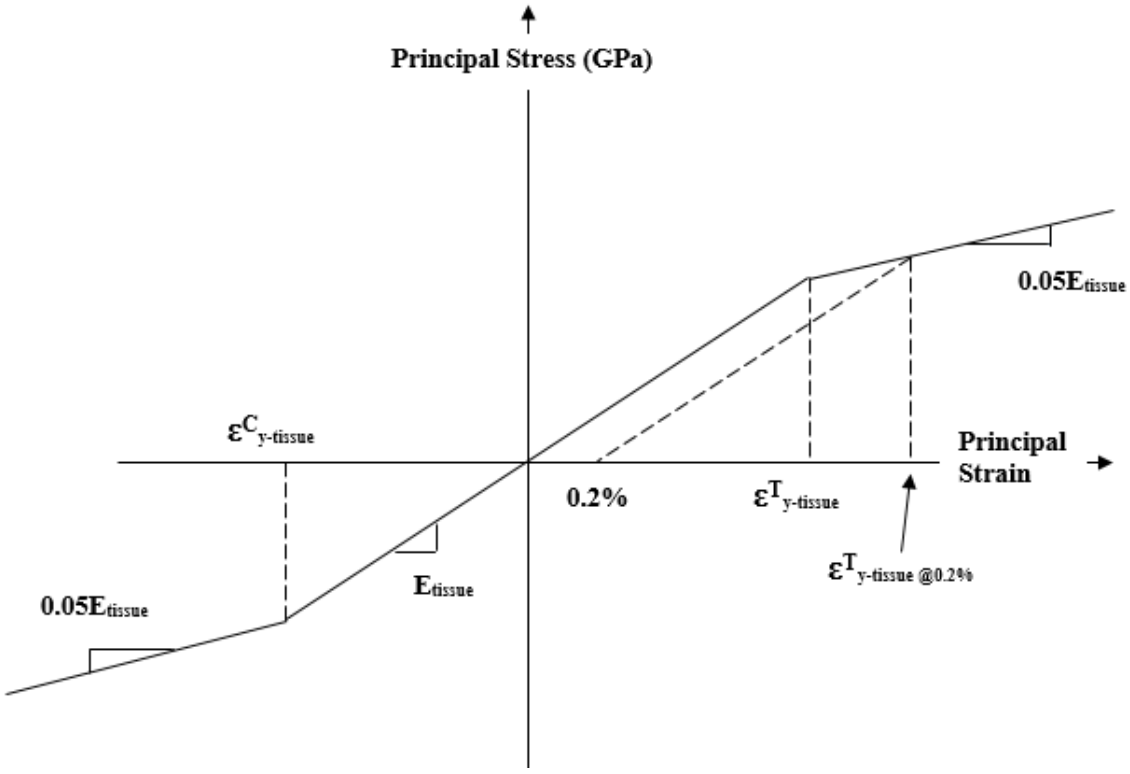

Figure 13: Bilinear elastic plastic model of trabecular bone tissue

Furthermore, experimental tensile and compression test results combined with Finite Element (FE) and curve fitting using regression analysis, estimated the pre-elastic modulus (E_{pre}) and post-elastic

modulus (E_{post}) to be E_{pre} =18.0 ± 2.8 Gpa and E_{post} = 5% of E_{tissue}. And the compressive yield strength (σ_y) to be σ_y= 135.3 ± 34.4 MPa. However, this result is obtained for a cadaveric human femoral trabecular bone tissue with varying amount of cortical tissue attached to it. A recent experiment conducted by Lakatos et. al. on several fresh cadaveric samples of mandibular trabecular bone gave the young's modulus ranging from 6.9 MPa to 199.5 MPa. These variations on the young's modulus is explained by the measuring techniques used and several physiological factors like the age, sex, effects of hormones, density, porosity, method of extraction, anatomical location, way of preservation and preparation of specimen. (Lakatos, Magyar, & Bojtar, 2014) A close relation between the apparent (i.e. homogenized) Young's Modulus (E_{app}) and apparent density (ρ_{app}) of the mandibular trabecular bone is given by the power law in equation 2-7 (O'Mahony, Williams, & Spencer, 2001), (Rho, Hobatho, & Ashman, 1995)

$$E_{app} = 2.349(\rho_{app})^{2.15} \qquad \text{(Eqn. 2-7)}$$

Where, ρ_{app} is in g/cm^3 and E_{app} is in GPa

Therefore, a similar analysis is needed to accurately estimate the pre, post and compressive yield strength for the gyroid network model that satisfy the result of Eqn. 2-7.

The table below shows various values of young's modulus of trabecular bones at different body parts. There are several variations in the young's modulus depending on the bone type, way of preservation of such bones before the experiment and the methods of experiments.

Author	Bone type	Preservation	Young's modulus
Evans and King, 1961 [15]	Femur	Embalmed	20.68–965 MPa
McElhaney et al., 1970 [16]	Vertebra	Fresh	Avg 151.7 MPa
Pugh et al., 1973 [17]	Femur	Frozen	423–1516 MPa
Schoenfeld et al., 1974 [18]	Femur	Fresh	Avg 344,7 MPa
Lindahl, 1976 [19]	Tibia	Dried, defatted	1.4–79 MPa
Lindahl, 1976 [19]	Vertebra	Dried, defatted	1.1–139 MPa
Carter and Hayes, 1977 [6]	Tibia	Frozen	10–500 MPa
Ducheyne et al., 1977 [20]	Femur	Frozen	58.8–2942 MPa
Brown and Ferguson, 1980 [21]	Femur	Frozen	1000–9800 MPa
Williams and Lewis, 1982 [22]	Tibia	Dried, defatted	8–457 MPa
Goldstein, 1987 [9]	Tibia	Frozen	4–430 MPa
Martens et al., 1983 [23]	Femur	Frozen	58–2248 MPa (900 ± 710 MPa)
Ciarelli et al., 1986 [24]	Tibia	Frozen	5–552 MPa
Ciarelli et al., 1986 [24]	Femur	Frozen	7.6–800 MPa
Ciarelli et al., 1986 [24]	Radius	Frozen	1.1–448 MPa
Ashman and Rho, 1988 [5]	Vertebra	Fresh	158–378 MPa
Keller et al., 1987 [25]	Vertebra	Frozen	15–30 MPa
Struhl et al., 1987 [26]	Vertebra	Frozen	10–428 MPa
Odgaard and Linde, 1991 [4]	Femur		103–1058 MPa
Linde, 1994 [3]	Tibia		445 ± 256 MPa
Keaveny et al., 1997 [27]	Vertebra		165 ± 110 MPa
Misch et al., 1999 [14]	Mandible	Frozen	24.9–240 MPa (with cortical layer) 3.5–125.6 MPa (without cortical layer)
O'Mahony et al., 2000 [13]	Mandible	Frozen	Avg 907 MPa (mesiodistal) Avg 511 MPa (buccolingual) Avg 114 MPa (inferosuperior)
van Eijden et al., 2004 [12]	Mandibular condyle	Embalmed	Avg 438 MPa (vertically) Avg 157 MPa (horizontally)
Chevalier et al., 2007 [10]	Femur	Dried, defatted	63.9–2987.9 MPa

Table 1: Experimental Young's Modulus values of trabecular bones obtained by different researchers

Source: (Lakatos, Magyar, & Bojtar, 2014)

2.4.1. Methodology

A bilinear elastic-plastic stress-strain diagram similar to the one in figure 13 was assumed for the material of the gyroid tissue. The post young modulus was set to (E_{post} =0.05 E_{tissue}), and the unknowns were taken as (E_{tissue}, σ_y). Therefore, the objective was to find the appropriate values of

(E_{tissue}, σ_y) such that the resulting characteristics equation of (E_{app} vs ρ_{app}) under compression is identical to that of equation 2.7 within 5% tolerance.

To achieve this objective in an efficient manner, the closed surface of a reference RVE of the gyroid network of total volume (TV = 2×2×2 mm^3) and bone fraction equal to (V_f =25%), was mathematically modeled using the Mathematica software (Wolfram.Inc) following the procedure described in section 2.3., the generated stereolithographic (STL) file was then imported to a solid modeling software (SolidWorks.Inc), and a solid model of the gyroid trabecular bone was formed using the software's Application Programming Interface (API) then stored a universal Parasolid (x_t) format. For consistency between (stl) and (x_t) models, the volume fraction was calculated using the measuring features of solidworks and the percent difference was less than (1%).

2.5. Discussion

The morphological properties like volume fraction, trabecular spacing, trabecular thickness and structural model index of a trabecular tissue is considered to develop a gyroid. This gyroid is minimal surface cellular solid that act as a morphological model of trabecular bone. This gyroid can be further varied in the volume fraction to obtain the necessary bone density. Its mechanical properties can be tested with a method of finite element analysis using ANSYS. Further, in this research we are determining the necessary composites required to resemble the properties of a gyroid which can be 3D printed and tested for young's modulus by performing compression test.

CHAPTER 3

DEVELOPMENT OF VERSATILE MODEL OF THE SCREW THREADED IMPLANT

3.1 Abstract

Tapered screw-type dental implants have been most commonly used while replacing a missing tooth. The bone to implant stability depends not only on the surface topology like nature of surface, thread profile, size, length and diameter of implant but also on the techniques involved like insertion torque, site preparation and the required micromotion. Lack of primary stability of the implant has resulted to almost 32% of the dental implant failure. An implant is usually divided into crown, screw, abutment and fixure. Design of this fixture and fabrication is going to be carried out with the availability of time and essential tools. At first we develop a versatile model of the screw-type model and then fabricate it using a mini CNC machine. Finally, we perform a pull out test where we measure the tensile strength necessary to dismantle the implant from the bone tissue. However, all the fabrication and testing parts are left out for future work.

3.2 Introduction

The success of dental implant replacements is based on their primary and extended stability within the host bone tissue. Traditional methods of the treatment would require a healing period of 3-6 months. Primary stability of dental implants is influenced by the quality and quantity of bone, the implant geometry, site preparation technique and the insertion torque. Even though, dental implants are the predictable phase of tooth replacement, higher than 10% of failure rate is still encountered which is usually because of soft bone quality and primary micro-motion. (Vidyasagar & Apse, 2004) Excess micro-motion immediately after dental implantation has the potential of protruding fibrosis and preventing implant-bone osseointegration. (Szmukler, Y, & Dubruille,

1998) A critical threshold of micromotion, which is not zero, is found to be between 50 and 150 microns as an early loading for a successful osseointegration. Lack of primary implant stability has resulted in a failure rate as high as 32% of the dental implants. (Friberg, Jemt, & U, 1991)

Secondary stability is the stability obtained upon the bone formation which is greatly influenced by the microscopic surface topography and macroscopic levels of implant designs. (Dows Institute of Dental Research, 1999) Dental implants manufacturers utilize a variety of surface treatment to favorable modify the implant surface roughness, chemical composition and potential existence of impurities. Considering these, it is possible to increase the contact surface and fixture strength between bones and implants even with highly porotic bones. (Vidyasagar & Apse, 2004)

The tertiary stability is the maintenance of osseointegration. The formation and stability of new bone around the implant is the combination of resorption and bone apposition. The balance between these processes is affected by various types of stimuli most notably, the biomechanical forces in the dental prosthesis environment and the potential presence of inflammation.

Tapered screw-shaped dental implants with various surface topologies (i.e. machined, acid etched, plasma sprayed, sand blasted, oxidized) and treatments, combining various materials, shapes, size, diameters, lengths and connections (Haas, Bernhart, Ortbudak, & Mailath, 1999) dominate the dentistry market. Increased surface topography results in increased bone to implant contact after the surgery, however, it might not increase the biomechanical interaction with bone. (Copper, 2000) Implants with relatively smooth surfaces have a higher failure rate than rough surfaces. A recent study conducted which uses oxidized implants to increase the surface study showed only a 3% failure rate while Glauser et. al. showed a failure rate higher than 17% for a machined implants. (Glauser, et al., 2003) Surface topography of implants might not contribute to the initial implant

stability, however, it reduces the risk of failure in secondary osseointegration and helps in quick wound healing.

Normally considered design principles of an implant would facilitate the following points:

1. To gain the initial stability by reducing the threshold for the tolerated micro motion
2. To reduce the effect of shear forces on the interface by incorporating various design factors
3. To stimulate bone formation and facilitate bone healing by incorporating bone healing

Thread profiles in an implant influence the initial stability, enlarge the implant surface area as well as, distribute the stress uniformly. (Brunski, 1988) The shape of the thread profiles (i.e. V-shaped, reverse buttress, square etc.) affects the magnitude of stress in the bone as Kohn et. al. found that the strain is concentrated in such areas where bone contacts the crest of thread and goes on decreasing towards the root. (Kohn, Ko, & Hollister, 1992) However, among various thread profiles, stress distribution is uniform in an asymmetric thread whose profile varies along the length of the implant. Highest bone stress is reported in the region of implant's neck meaning the implant's neck should be smooth and polished. However, studies showed a significant crestal bone loss due to smooth implant neck and proved a shorter and rough implant neck to induce a favorable stress on the bone. (Branemark, et al., 1977) A successful implant designs require careful manipulation of the implant geometry and material together with realistic testing on substrates which serves a patient specific bone.

3.3 Design of a Versatile Dental Implant

A schematic diagram of the endosseous implant profile is shown in figure 14, the implant total length was sectioned into four separate lengths. The abutment was set at a fixed length of (L_1) and inclination (α). The section in contact with the cortical bone was characterized by its uniform

cross-sectional radius (r_2) and variable length (L_2), the thread pattern and cross-sectional profile within this section satisfy respectively, the characteristic equations of the fixed pitch helix in equation 3-1 and that of the closed curved shape in equation 3-2. Figure 15 describes the local coordinate system used in Eq.3-2.

$$\begin{cases} x = r_2 \cos(\omega\, t) \\ y = r_2 sin(\omega\, t) \\ z = \left(\frac{L_2}{2\,\pi}\right) t \end{cases}, \quad (0 \le t \le 2\pi) \tag{3-1}$$

$$\left(\frac{x'}{a}\right)^p + \left(\frac{y'}{a}\right)^p = 1 \tag{3-2}$$

The majority of the implant length is embedded within the cancellous bone

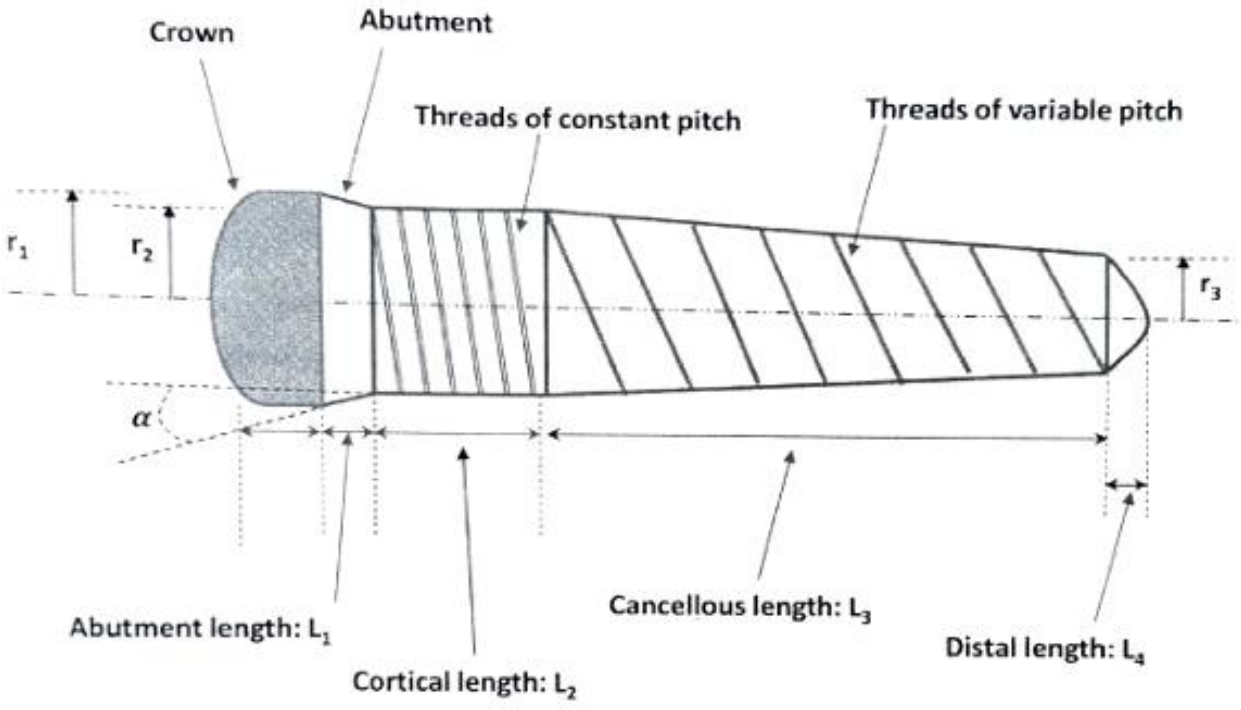

Figure 14: Implant Parametric Profile

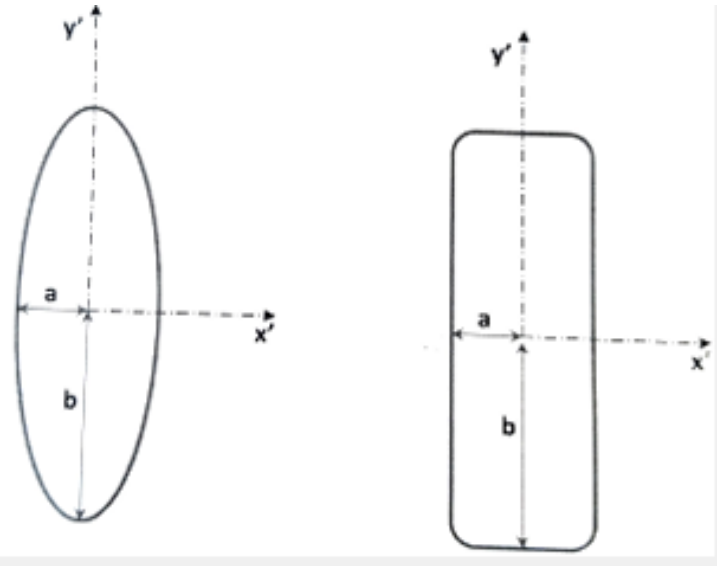

Figure 15: Thread profile following equation 3-2, for a ≠ b and [(1:p=2), (2:p=4)]

3.4 Discussion

All the necessary literature reviews, design of the implant which can show highest range of stability with varying strength of oesteoporotic bone, its fabrication and the testing part are not performed in this research and this part is assigned for future work.

CHAPTER FOUR

3D PRINTING AND EXPERIMENTAL VERIFICATION OF MECHANICAL PROPERTIES OF TRABECULAR BONE

4.1 Abstract

3D printing is a very easy and adaptive method to produce prototypes using easily available materials like ABS, PLA etc. As a very first approach we mixed definite proportion of pure ABS with 30% GF ABS to produce the desired composition of GF ABS. Since the mixing of LLDPE is not feasible as the 3D printer couldn't extrude the filament we limit our composition to ABS and GF ABS only. The weighed proportion of composition were mixed in a mixer for 2 hours to ensure homogenous mixture and was extruded through bench type filament extruder. Those filaments were used to print our samples and was compression test was performed to find the young's modulus of each sample. Experimentally we are trying to verify the mechanical properties of the trabecular tissue which varies from 6 MPa to 18 GPa (Bayraktar, et al., 2004) (Lakatos, Magyar, & Bojtar, 2014) all depending on the nature of sample, its origin, fabrication and experimental procedure. Our test results varies from 900 MPa to 2200 MPa for different composition of samples. And the results for the gyroids resembling trabecular bones are still lower around 1900 MPa which is basically because of the inconsistency in experimental procedures.

4.2 Introduction

Three-dimensional (3D) printing is very adaptable and innovative process which brought revolution in additive manufacturing (AM) techniques to create 3D objects. Fused Deposition Modelling (FDM) is a rapid prototyping process that produces prototypes from materials like PLA, ABS, PETG etc. where it lays semi-molten plastic filaments through the nozzle onto a plate-form, layer by layer to get the desired object. (Zixiang, Jianlei, Senthil, & Lixin, 2016) Generally, it uses

a spool of thermoplastic filament which is then melted inside a printing nozzle barrel and the resulting liquid plastic is laid down layer by layer. Because of its simplicity in use, cheap cost, and environment-friendly features, FDM is commonly used for non-industrial desktop 3D printers. Most of the products and the prototypes produced from FDM can directly be used as several industrial accessories, household appliances, medical appliances, toys and aesthetic purposes. (Lee, Abdullah, & Khan, 2005) However, there are several shortcomings despite its worldwide use. Mechanical properties of the printed prototypes usually varies because of the printing conditions like temperature, layer height, air gaps etc. some of which, we will go in details on later sections. A study done by Sung et al. (2002) suggested that the tensile strength of the parts produced from FDM ranges between 65 and 72 percent to that of the strength of parts made from injection modeling while the compressive strength ranged from 80 to 90 percent for the injection modeled FDM. (Sung, Michael, Dan, Shad, & Paul, 2002)

4.3. 3D Printing of Gyroid

4.3.1. Build Parameter Considerations

First step before printing the gyroid and thereafter conducting the experiment was to identify the process control parameters which affects the properties of FDM prototypes. Some of the parameters are described below.

Infill: Infill shows how much a solid model should be filled in with the printing materials when printed. It is represented in percentage, 0 being no infills while 100 being the maximum that creates a solid compact part. For normal use 20-30% infill is enough, however, if we want optimal strength we can increase this value. There are several infill patterns such as rectilinear, grid, triangular, wiggle, fast honeycomb, full honeycomb etc. It influences the print weight, material usage,

strength and print time. For the purpose of this research a 100 percent grid infill was selected since we want the maximum strength possible.

Layer Height: Layer height is the vertical dimension or the dimension in Z-axis of each extruded bead/layer and it will affect the smoothness of the parts. Selecting lower layer height is ideal for smoother finish however it will take considerable amount of time to finish a job. Standard layer height usually lies between 0.01mm to 0.3mm. For the purpose of this research we have selected a layer height of 0.2mm.

Layer Thickness: Layer height and layer thickness are sometimes considered as same. Layer thickness normally known as bead width is the thickness of the bead that a FDM nozzle deposits. Layer thickness for ABS is taken between 0.18- 0.25 mm. Thick layers tend to produce a stronger part but at the same time there is a significant increase in temperature which causes delayed time for each layer to bond and this causes blobs in the top layer. For the purpose of this research we have considered a layer thickness of 0.2mm.

Air Gap: Air gaps are the distance between the two adjacent layers/ beads. An air gap of zero means the two adjacent beads just touch each other leaving no space between then. This is considered when we want a dense and strong parts and as the air gap value goes on increasing the gap increases and we can find loosely packed structures.

Bed Temperature: Bed temperature plays a significant role in 3D printing as it prevents deformation of specimen after a sudden cooling. In order to prevent wrapping which is caused due to quick cooling and to get an initial firm layer the printing platform is always kept heated to a suitable temperature. The recommended temperature for the heated bed lies between 80^0C to

100^0C for ABS and between 65^0C to 75^0C for PLA. For a successful print the first few layers are printed usually at 5^0C to 10^0C higher bed temperature than the successive layers.

Extruder Temperature: It is also commonly known as build temperature or nozzle temperature which is the temperature of the heating element. It controls the viscosity of the molten material extruded from the nozzle. Different materials have different build temperature. ABS is commonly extruded at a temperature between 220^0C to 250^0C. Sometimes it is necessary to change the extruder while printing composite materials since they require higher temperature to melt.

Printing Speed: Speed can affect the quality of the finished product. Low speeds are generally considered for the best results if the print has a lot of details. Printing gyroids at a higher speed causes layer separation, incomplete layers, rough corners and overall poor quality of the product. ABS filament, however, can be printed at relatively higher speeds usually above 70 mm/s but it is required to increase the nozzle temperature to keep the ABS hot enough to be printed uniformly.

Other than these, for a successful 3D print we need to make sure the heated bed is clean and dust free, the filament be clean, proper use of cooling fan depending on the type of printing materials used, nozzle diameter, extrusion speed, proper use of adhesion on the print bed, use of rafts and skirts to start a wrapping free print and possible use of supports while printing large and complex objects.

4.3.2. 3D Printing Materials

Acrylonitrile Butadiene Styrene (ABS)

ABS has a low melting point which makes it ideal for 3D printing. The acrylonitrile in ABS provides chemical and thermal stability, butadiene helps in toughness and strength while styrene provides rigidity and processability and gives the polymer a nice, smooth finish.

Natural white ABS pallets were purchased from IC 3D Industries. Two 3lb jar pure ABS pallets were enough to produce the required filaments. These pallets were later mixed with 30% GF ABS in certain proportion to get the desired composition.

Figure 16: IC 3D ABS pallets used for extruding filament

Glass Fiber Reinforced ABS: A glass fiber reinforced ABS gives higher tensile strength and higher modulus than pure ABS. A 30% glass fiber reinforced ABS was bought from Xiamem Keyuan Plastic Co. Ltd. China. Since the company do not sell the volume in small jars, we bought a 25 kg sack of 30% glass fiber reinforced ABS.

Linear Low Density Polyethylene (LLDPE): Linear low density polyethylene is a very softer and flexible form of plastic. It can absorb impacts and has great strength without being tearing. It has better tear and impact strength than LDPE (low density polyethylene) and HDPE (high density polyethylene). In this experiment we are trying to mix LLDPE with GF ABS so that the extruded filament can be easily 3D printed since only using GF ABS produces very brittle filament which is easily breakable.

Figure 17: 30% GF ABS and LLDPE used for printing filament

4.3.3. Preparation of Composites

Pure ABS and the 30% glass fiber reinforced ABS were mixed in different proportion by weight to produce 5%, 6%, 7.5%, 9%, 10%, 12%, 15% and 17% glass fiber reinforced ABS. To make 5% GF ABS, 5 portion by weight of pure ABS pallets was mixed with 1 portion by weight of 30% GF ABS pallets. To make 6% GF ABS, 4 portion by weight of pure ABS pallets was mixed with 1 portion by weight of 30% GF ABS pallets. Likewise, to make 7% GF ABS, 3.285 portion by weight of pure ABS pallets was mixed with 1 portion by weight of 30% GF ABS pallets. And to make 7.5% GF ABS, 3 portion of pure ABS pallets was mixed with 1 portion by weight of 30% GF ABS pallets. Similarly, 8% , 9% and 10% GF ABS were made by mixing 2.75 portion by weight, 2.33 portion by weight and 2 portion by weight of 30% GF ABS pallets respectively. And to make 12%, 15% and 17% GF ABS ,1.5 portion by weight, 1 portion by weight and 0.76 portion by weight of pure ABS was mixed with 30% GF ABS.

Figure 18: OHAUS beam balance weighing apparatus used for measuring the weight of pallets

The table below shows the composition of the pure ABS and GF ABS mixed to produce required composition.

S.N.	Pure ABS by weight	30% GF ABS by Weight	Produced GF ABS Composition
1.	5	1	5% GF ABS
2.	4	1	6% GF ABS
3.	3.285	1	7% GF ABS
4.	3	1	7.5% GF ABS
5.	2.75	1	8% GF ABS
6.	2.33	1	9% GF ABS
7.	2	1	10% GF ABS
8.	1.5	1	12% GF ABS
9.	1	1	15% GF ABS
10.	0.76	1	17% GF ABS

Table 2: Weight proportion of pure ABS and 30% GF ABS mixed to get desired percentage of composition

The following table shows the properties of ABS, 30 % glass fiber reinforced ABS, 10% glass fiber reinforced ABS and LLDPE used for the experiment. (MatWeb LLC, 2019)

S.N.	Properties	ABS	30% GF ABS	10% GF ABS	LLDPE
1.	Elastic Modulus	1.79 – 3.2 GPa	3.3 – 10 GPa	2.5 - 5.88 GPa	0.14 – 1.57 GPa
2.	Tensile Strength	20 – 77 MPa	38- 117 MPa	28 – 88 MPa	7.58 – 19 MPa
3.	Compressive Strength	55 – 70 MPa	104 –117 MPa		
4.	Melting Temperature	210 – 270^{0}C	160 – 288^{0}C	188 - 275^{0}C	95 – 302^{0}C
5.	Extrusion Temperature	210 – 240^{0}C	204 – 238^{0}C	193 – 232^{0}C	149 – 205^{0}C
6.	Density	0.9-1.53 g/cm^3	1.17-1.5 g/cm^3	1.06-1.40 g/cm^3	0.91-1.01 g/cm^3

Table 3: Properties of pure ABS, 10% GF ABS, 30% GF ABS and LLDPE

After the necessary proportions of quantities are determined, they are mixed in a V shaped powder mixing chamber. We can continuously rotate the chamber or can assign the time until which the chamber rotates mixing the materials inside. To ensure a uniform mixing of the pure ABS with GF we rotated the chamber for at least two hours for each composites samples.

Figure 19: V-shaped mixing chamber used for mixing the calculated amount of pure ABS and 30% GF ABS

4.3.4. Preparation of Filament

A Wellzoom Desktop Extruder was used for the purpose of filament extrusion. This extruder is designed for non-professional operators and can easily be used in laboratories because of its light weight and portability. Extruding filament made from composite materials with low risk of mis-operation is the key advantage to have used this extruder for the purpose of this research.

The composite pallets after mixing in the V shaped chamber is put into the hooper of the single screw extruder of diameter 1.75mm. We set the extrusion temperature to 180^0C for extruding pure ABS and to 190^0C for extruding the GF reinforced ABS since it's the melting temperature is higher than pure ABS. There is always some residue at the nozzle of the extruder hence we threw initial approximately two meters of extruded filament to ensure correct composite materials. Also few meters of the lately extruded filaments are not used since there is very less amount of composites

inside the hooper due to which the filament is not uniform in composition and diameter. Each time we put new proportion of composites we threw the initial few meters of filament to bring the uniformity. We prepared several spools of filament of various composition and marked them so that we would not use wrong filament while 3D printing.

Figure 20: Wellzoom desktop filament extruder

4.3.5. 3D Printing

The extruded filament were used to print the models. At first, a solid cube of 10mm × 10mm × 10mm for various percentage of composition were printed. Ten samples of each of such cubes were printed and the worst pieces were not used. A convenient printing setup while printing the models used were a nozzle temperature of 235^0C, bed temperature of 100^0C, extrusion speed 75%, flow 100%, infill of 100% and nozzle diameter of 0.4mm. Pure ABS samples were printed using normal low temperature head extruder which uses brass nozzles of 0.4 mm while, for composites, a high temperature head extruder which uses steel nozzle of 0.4mm was used since the GF

composites can easily erode the brass nozzle and during which a higher temperature is generated which a low temperature head extruder cannot withstand. For proper adhesion on the bed plate, Elmer's glue sticks were used since it is easily washable after the print and is also recommended by many professionals.

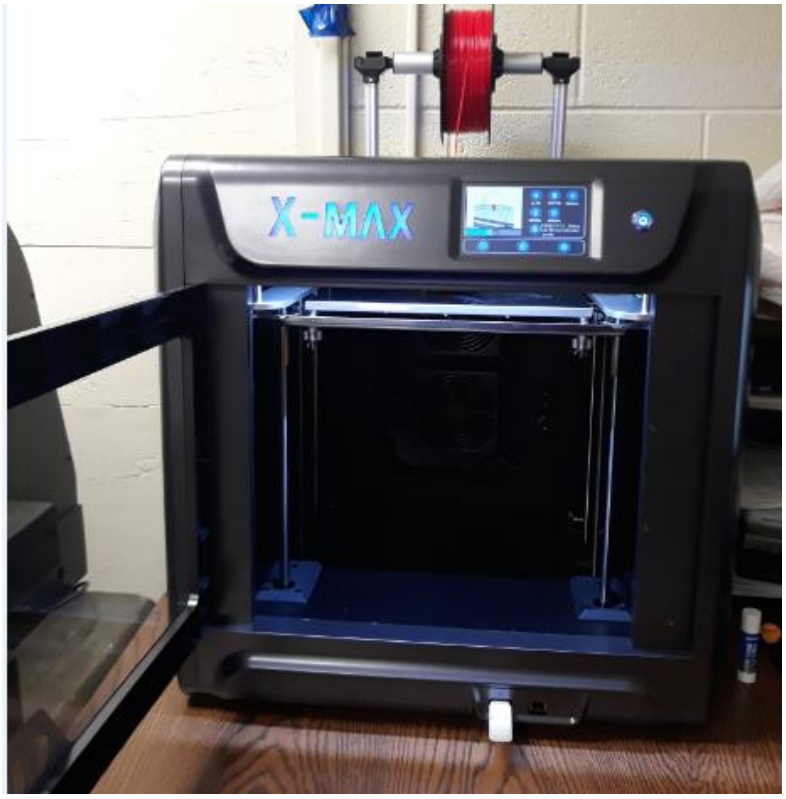

Figure 21: QIDI X-MAX 3D printer used for printing samples

4.3.6. Test Setup

The specimens for mechanical studies of 3D printed samples were designed according to ASTM D625 however, few geometrical criteria are omitted for the ease of printing but the test was conducted accordingly. First, we printed solid cubes of dimension 10mm ×10mm ×10mm of varying percentage of composites in 3D printer using high performance extruder. Those samples were allowed to cool down in room temperature and marked accordingly to keep the record.

*Figure 22: Test samples of dimension 10*10*10 mm to determine the young's modulus*

We desire to 3D print the test samples of dimension 10×10×10 mm however, each time we print the samples they are off the desired dimension because of printing conditions. Accurate measurement of dimension of each samples are tabulated in table 4.

All dimensions are in millimeter (mm)

S. N.	5%			6%			7.5%			9%		
	L	B	H	L	B	H	L	B	H	L	B	H
1.	10.4	10.2	9.9	10	10.1	9.7	10.2	10.4	9.7	10.1	9.9	9.7
2.	10.1	10.1	9.8	9.8	10.1	9.8	10.2	10.3	9.8	9.9	10.2	9.7
3.	10.4	10.2	9.9	9.9	10.1	10	10.4	10.2	9.7	10.2	9.9	9.8
4.	10	10.1	9.8	10.2	10	9.9	10	10.1	9.8	9.9	10	9.7

5.	10.2	10	9.8	10.2	10.1	9.8	10.4	10	9.8	9.9	10	9.7
6.	10.2	10	9.8	10	10.1	9.8	9.9	10.3	10	10	9.8	9.7
7.	10.1	10.4	9.8	9.9	10.2	9.9	10.2	9.8	9.7	10	10.2	9.7
8.	10.1	10.1	9.9	10	10.1	9.8	9.9	10.3	9.7	10	9.9	9.7
9.	10	10.1	9.9	10.1	10	9.8	10.2	10	9.7	9.9	10.2	9.7
10.	10	10.3	9.7	10.1	10	9.7	10.1	10.2	9.7	10.1	9.9	9.8
S. N.	10%			12%			15%			17%		
	L	B	H	L	B	H	L	B	H	L	B	H
1.	9.9	10.2	9.7	10.4	10.3	10	10.1	10	9.9	10.2	10	9.8
2.	10	10.1	9.9	10.3	10.2	9.9	10.1	10.2	9.8	10.1	10.1	9.7
3.	9.8	10.2	9.8	10.3	10.2	9.9	10.3	10.2	9.9	10.	10.2	9.9
4.	9.8	9.9	9.7	10.2	10.2	9.8	10.4	10.1	9.8	10.3	10.3	9.9
5.	10	10.1	9.7	10	10.1	9.7	10.2	10	9.7	10.4	10.1	9.9
6.	10.1	10	9.7	10.1	10.4	9.7	10	10	9.7	10.1	10	9.7
7.	10	10.3	9.7	10.2	10.1	9.9	10.1	10	9.9	10.2	10.3	9.8
8.	10.2	10.3	9.9	10	10	9.8	10.1	10.2	9.8	10.1	10.2	9.9
9.	10	10	9.9	10.3	10.2	9.8	10.3	10.4	9.8	10.	10.1	9.8
10.	10.1	10	9.9	10.2	10.3	9.8	10.3	10.2	9.9	10.3	10.2	9.9

Table 4: Accurate measurement of dimension of each test samples before compression test

Each samples were tested for compression in a modified dynamic load tester. The testing machine is programmed to be controlled in speed and in load and we have the option to provide the dimension of our test specimen.

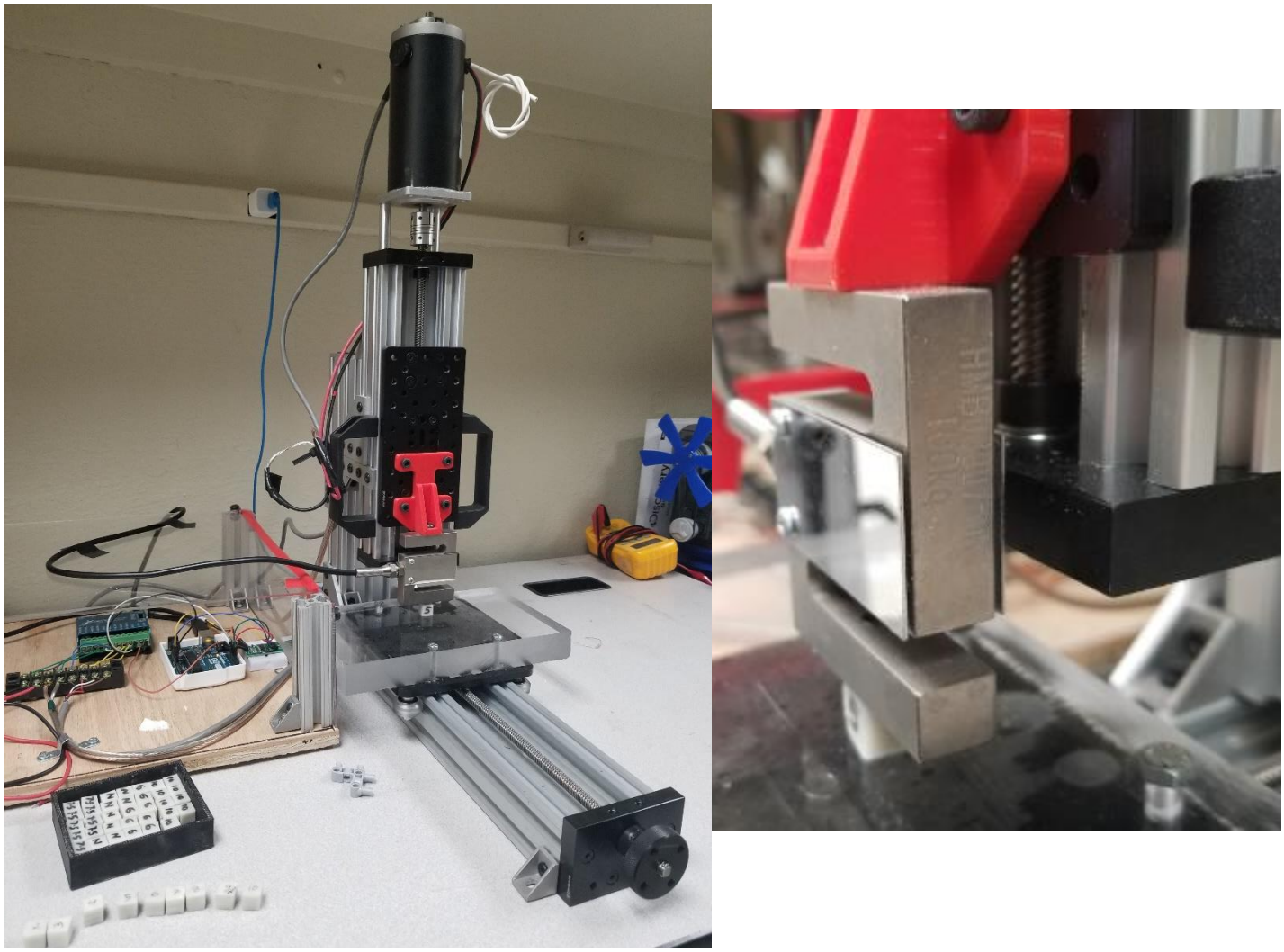

Figure 23: Dynamic load tester used for compression test of samples which is programmed to apply variable load

After the compression tests are performed, dynamic load tester automatically plots the graph of force against displacement and stress against strain. The stress-strain plots for the most successful tests are shown in the results and discussion section.

4.4. Results and Discussions

Following is the plot of stress against strain for samples of 5% GF-ABS composition.

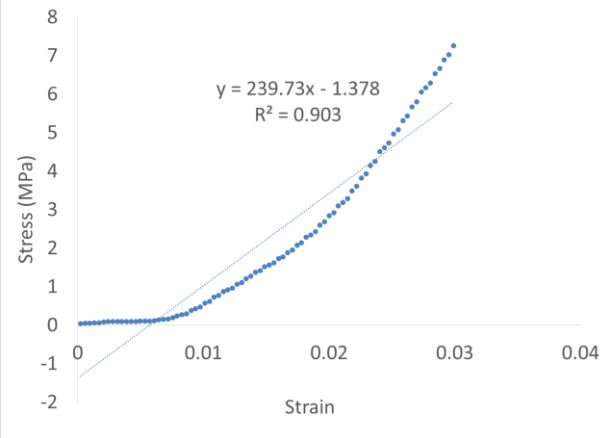

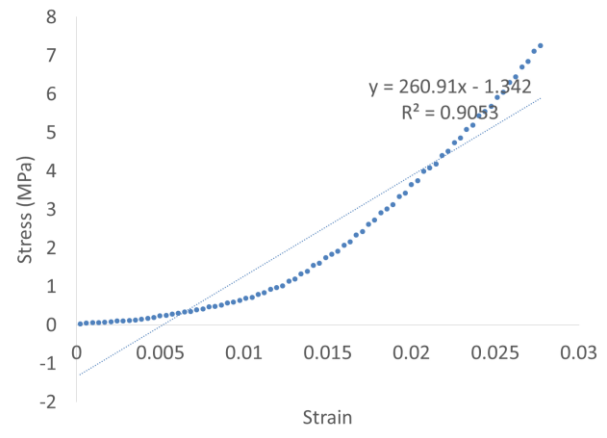

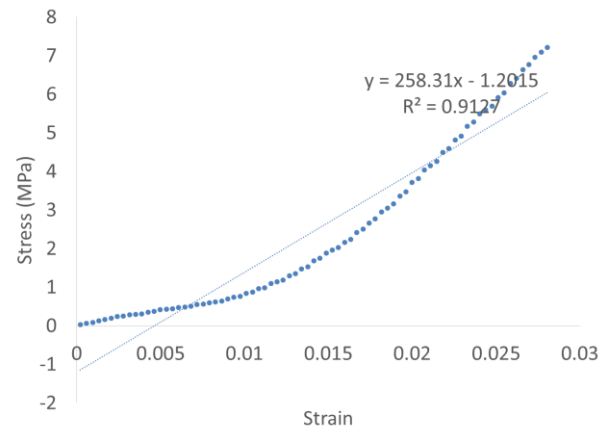

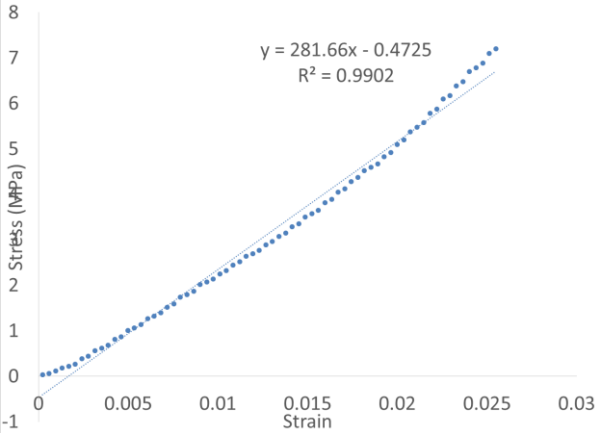

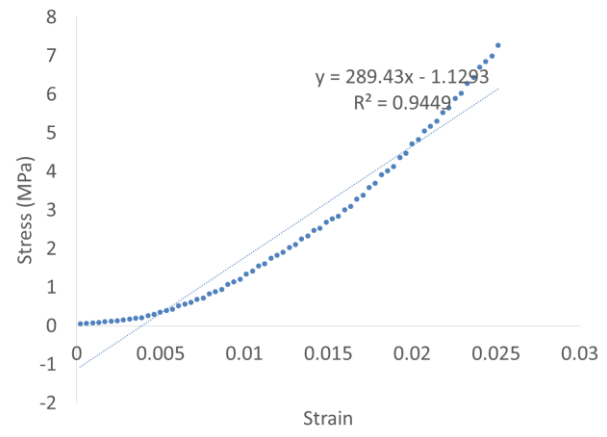

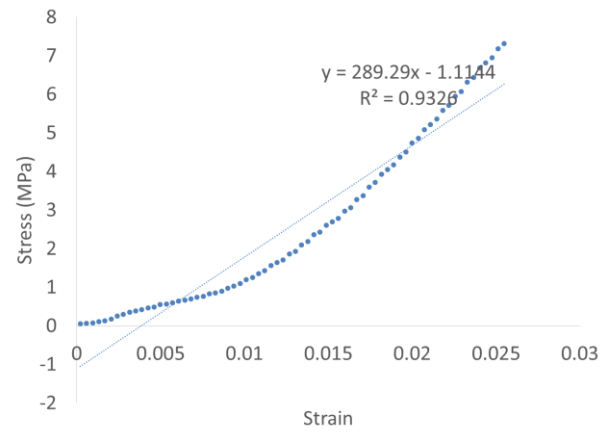

Following is the plot of stress against strain for samples of 6% GF-ABS composition.

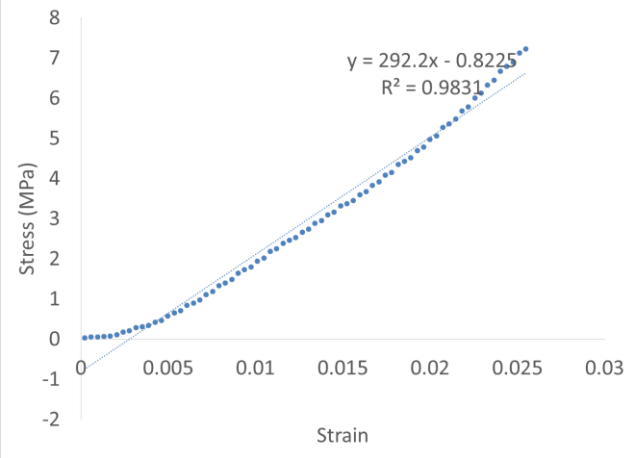

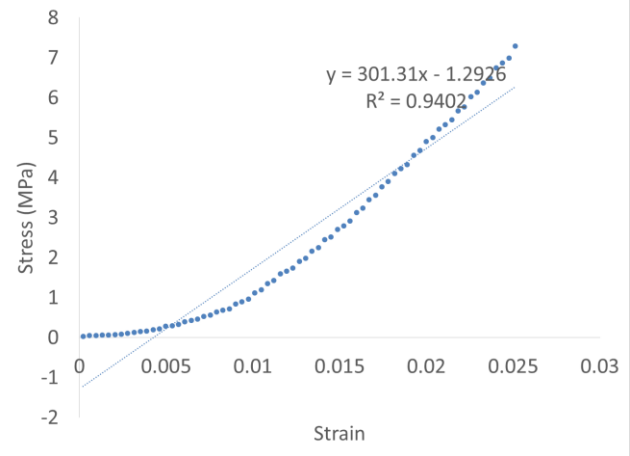

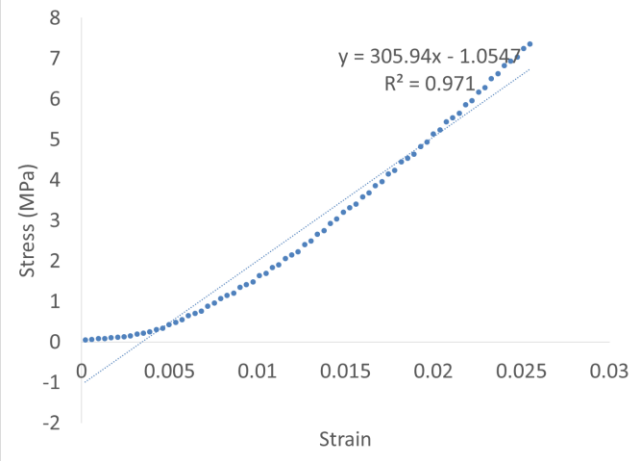

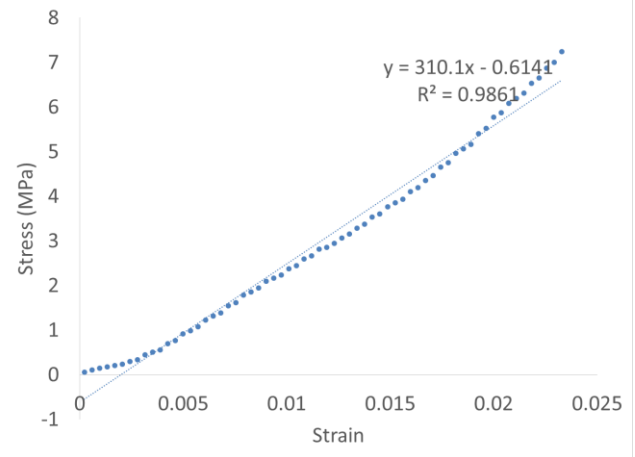

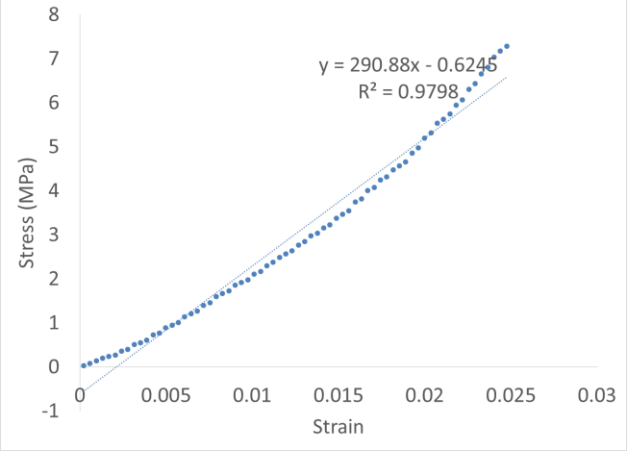

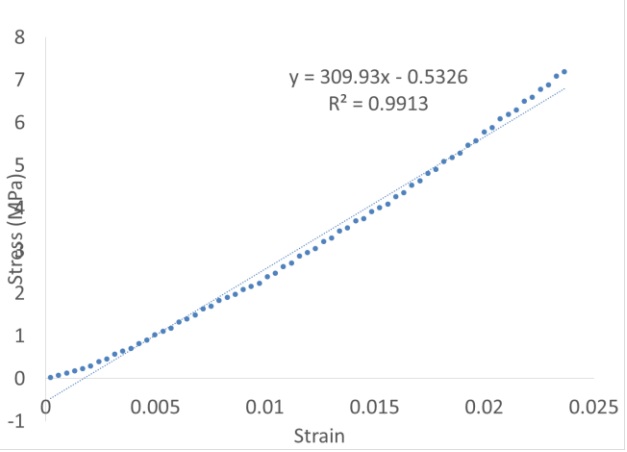

Following is the plot of stress against strain for samples of 7.5% GF-ABS composition.

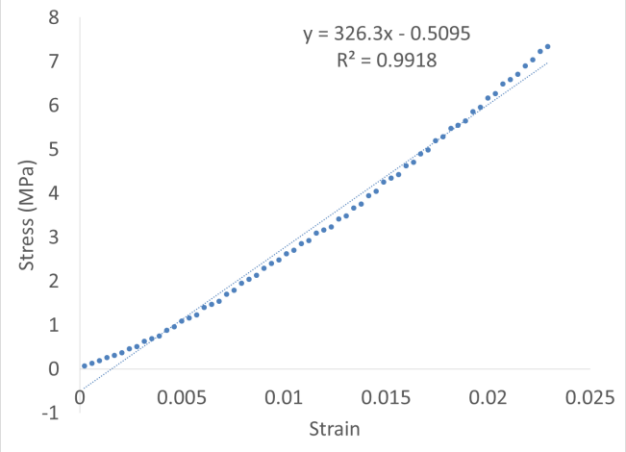

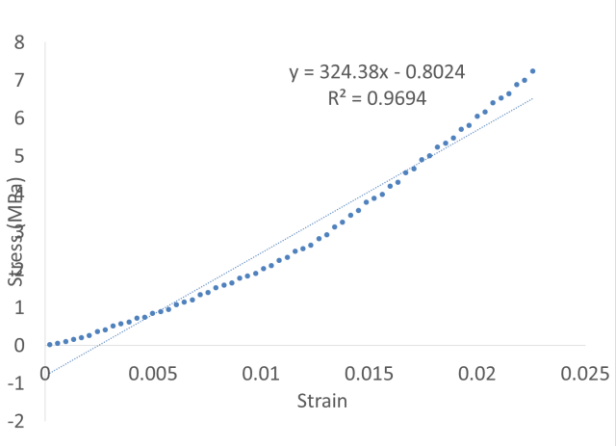

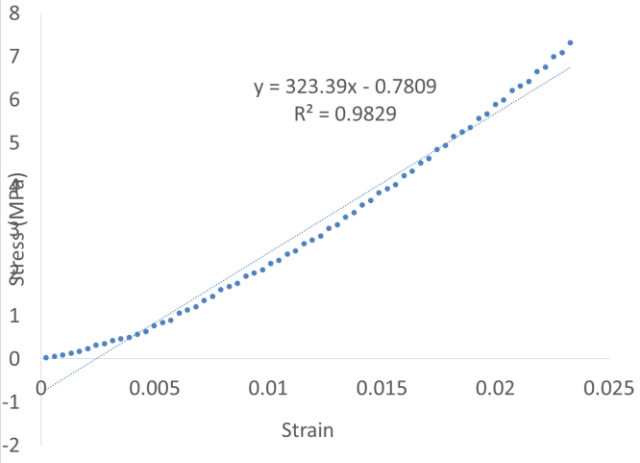

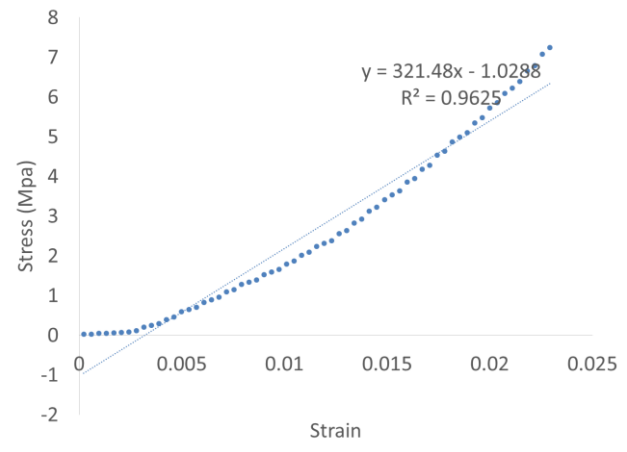

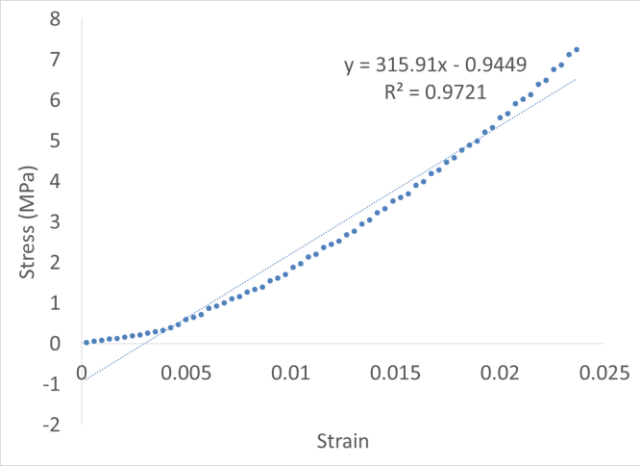

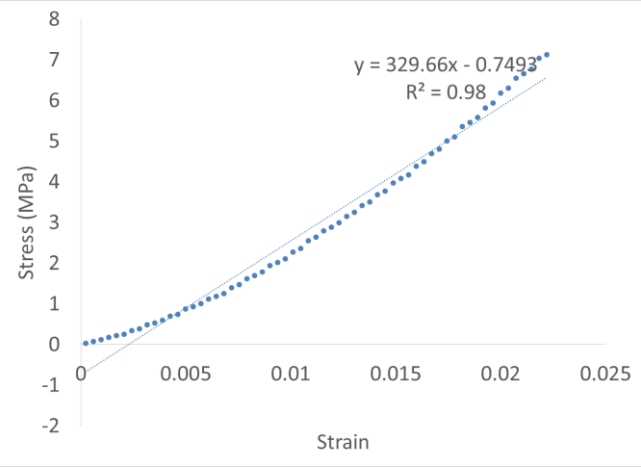

Following is the plot of stress against strain for samples of 9% GF-ABS composition.

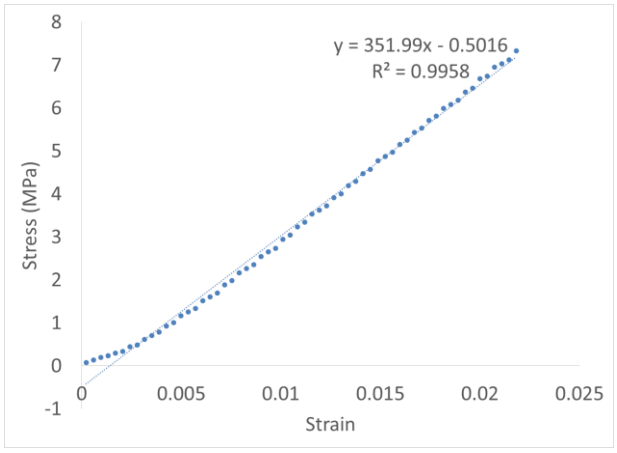

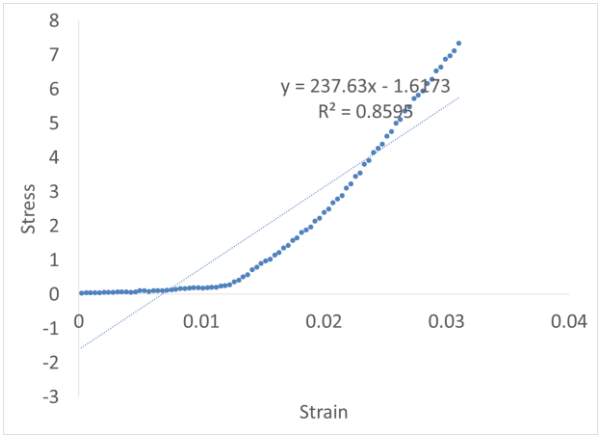

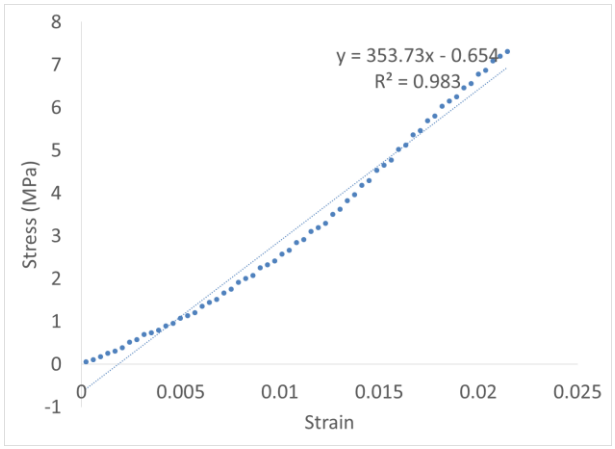

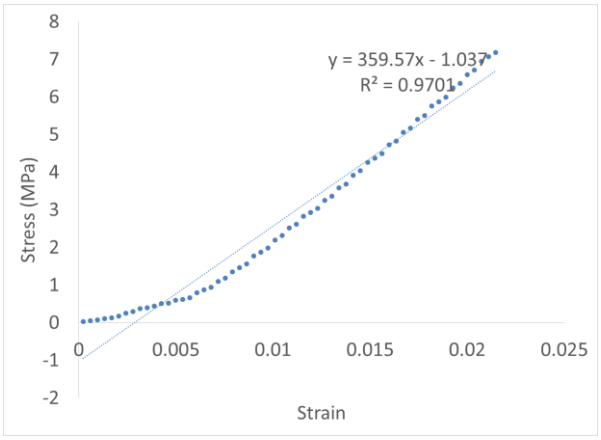

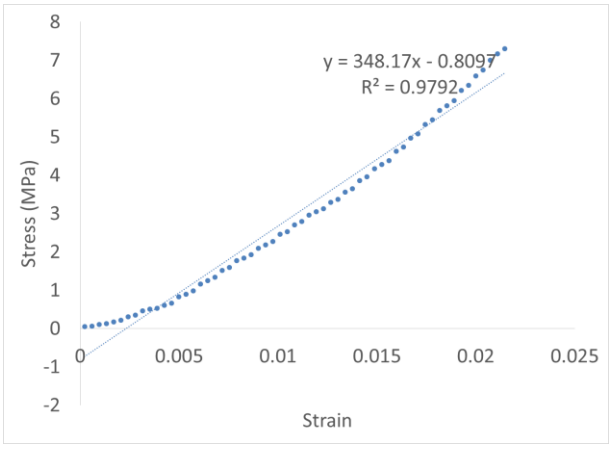

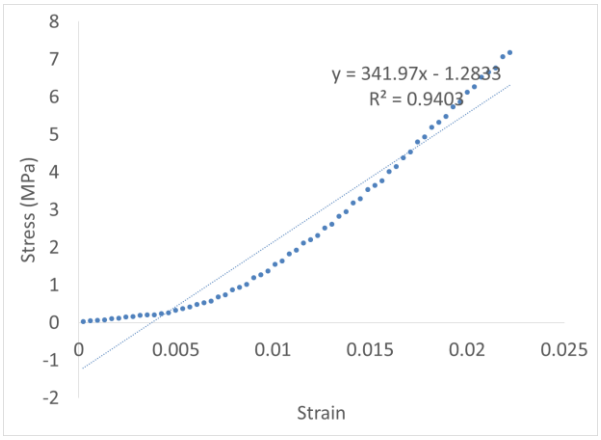

Following is the plot of stress against strain for samples of 10% GF-ABS composition.

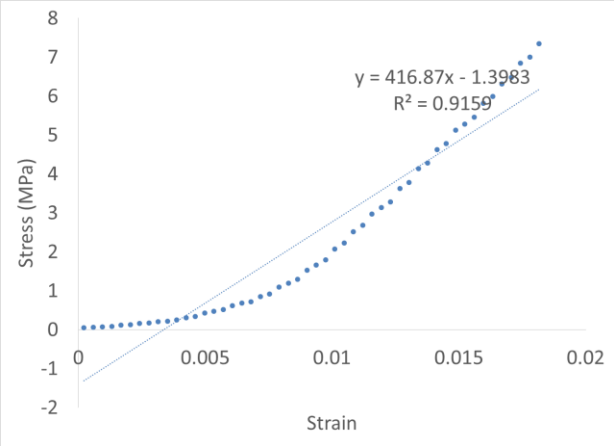

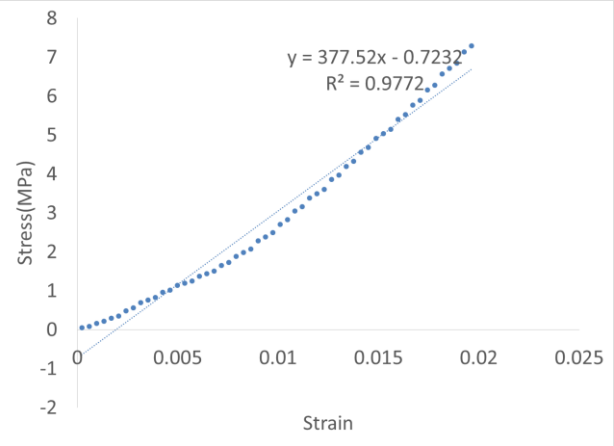

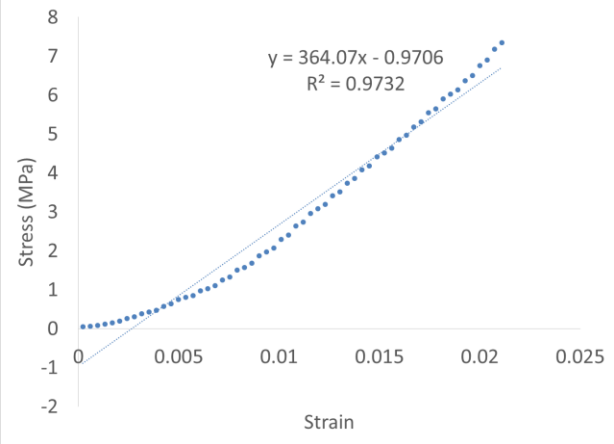

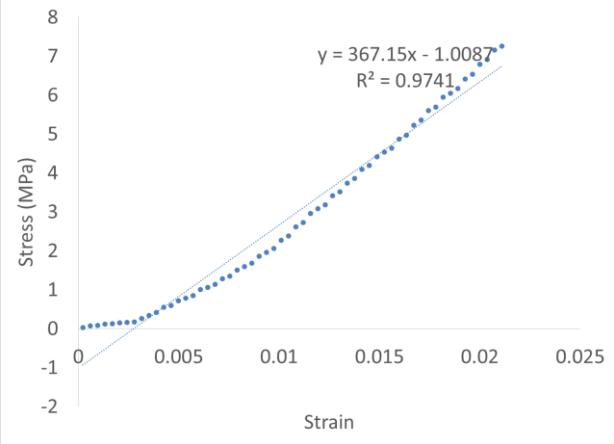

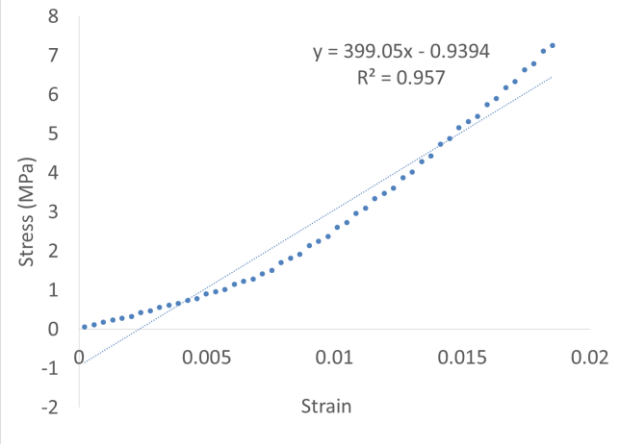

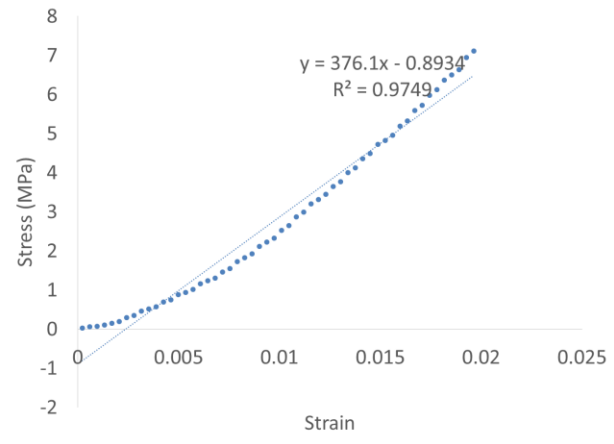

Following is the plot of stress against strain for samples of 12% GF-ABS composition.

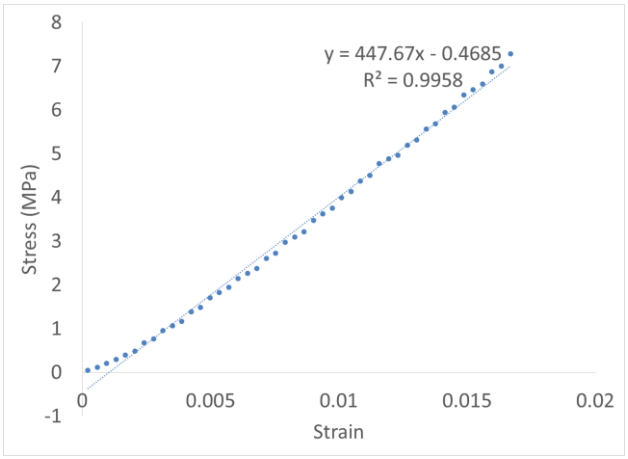

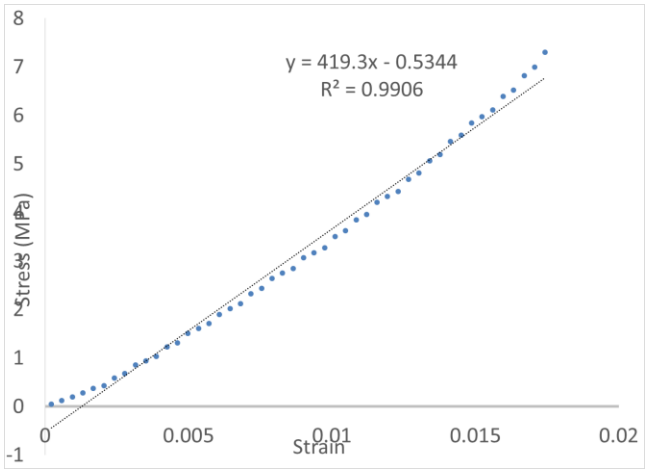

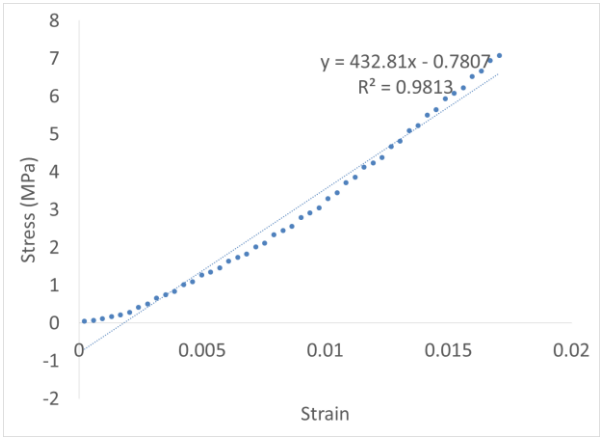

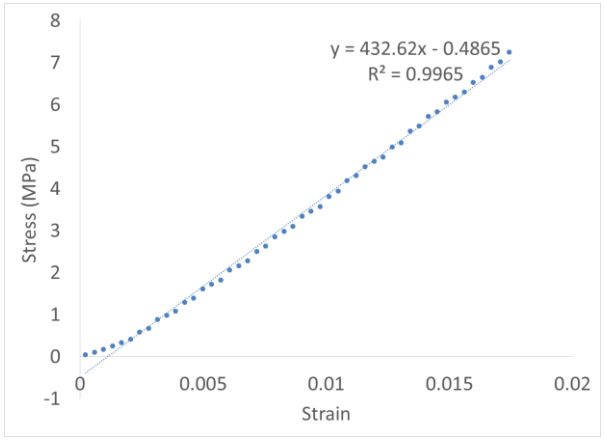

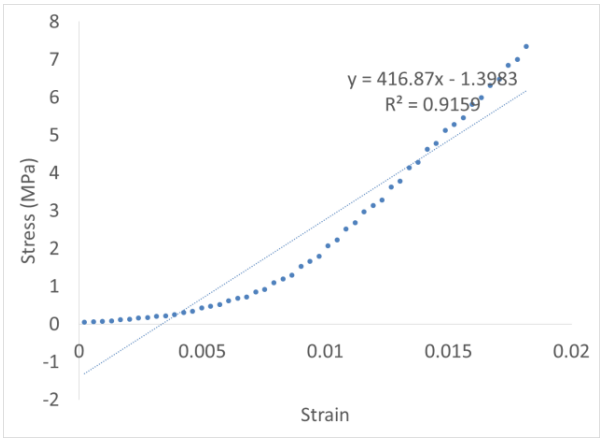

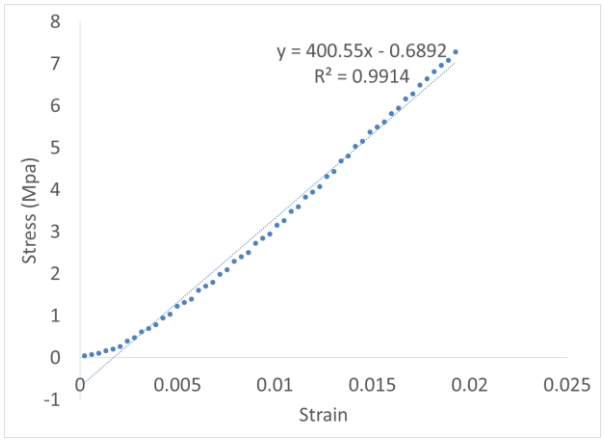

Following is the plot of stress against strain for samples of 15% GF-ABS composition.

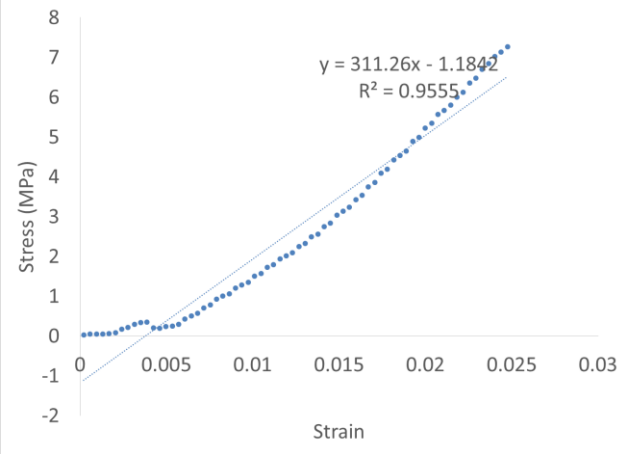

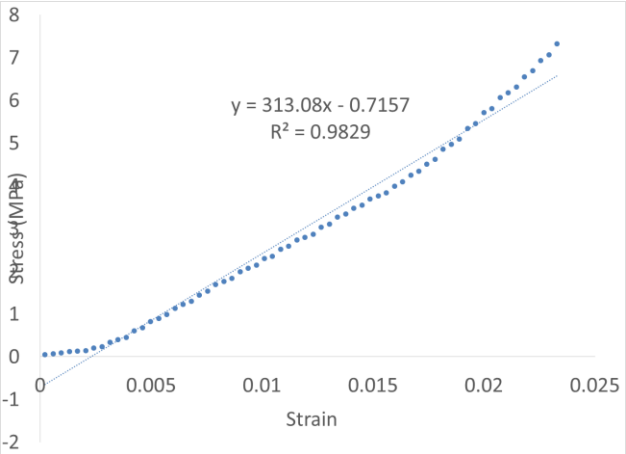

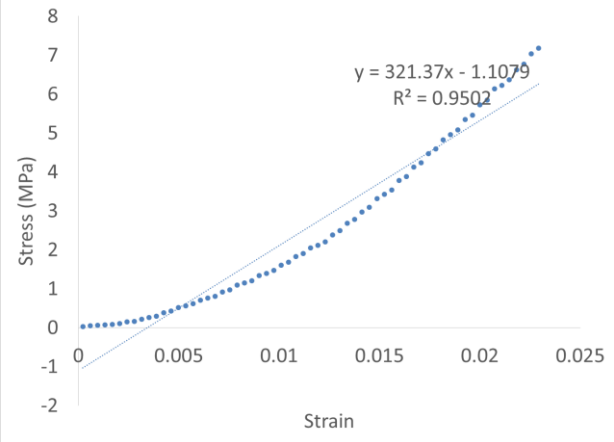

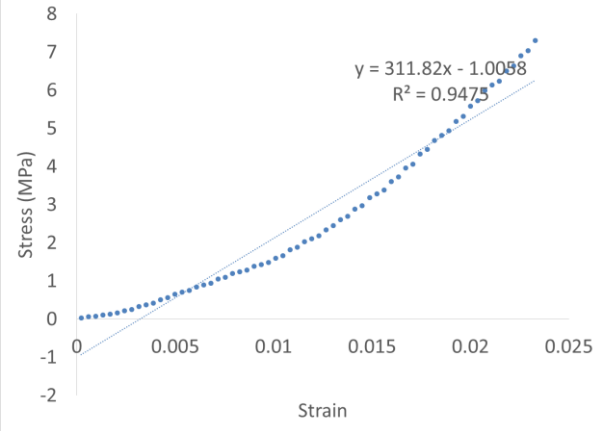

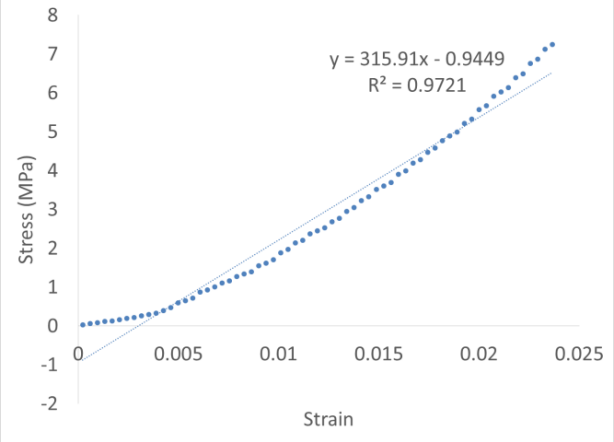

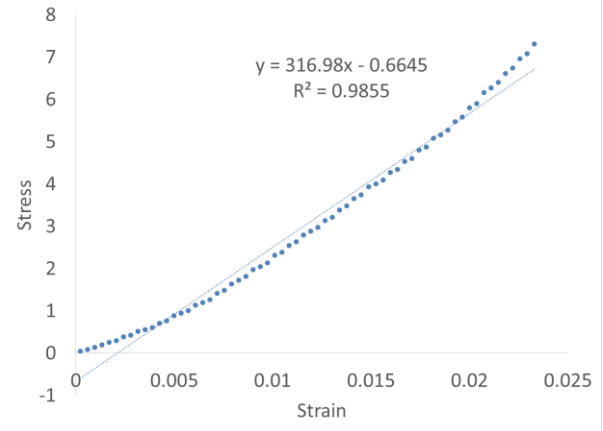

Following is the plot of stress against strain for samples of 17% GF-ABS composition.

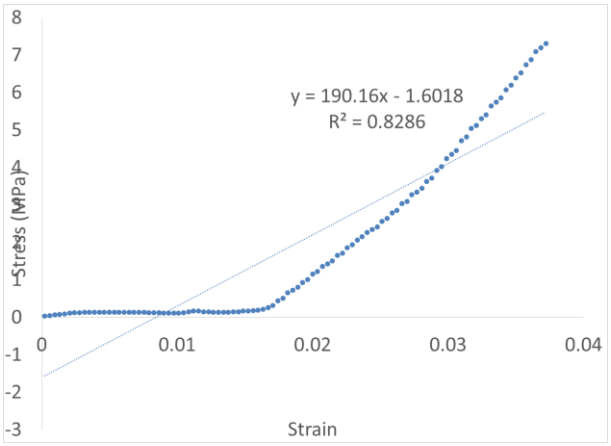

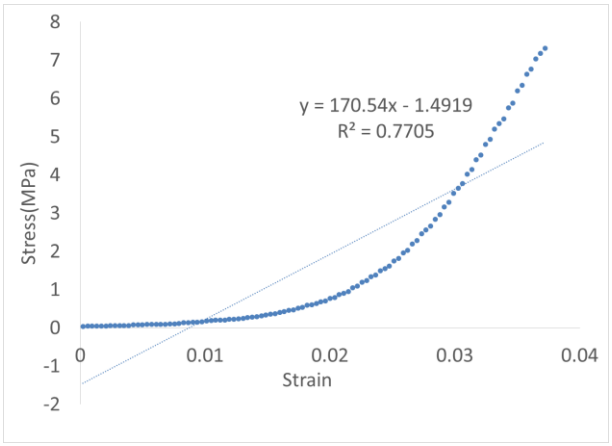

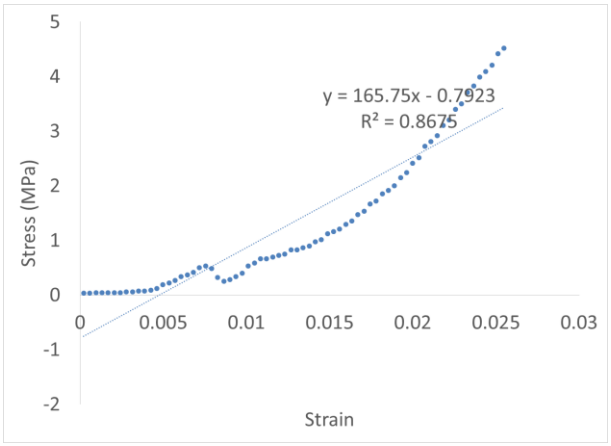

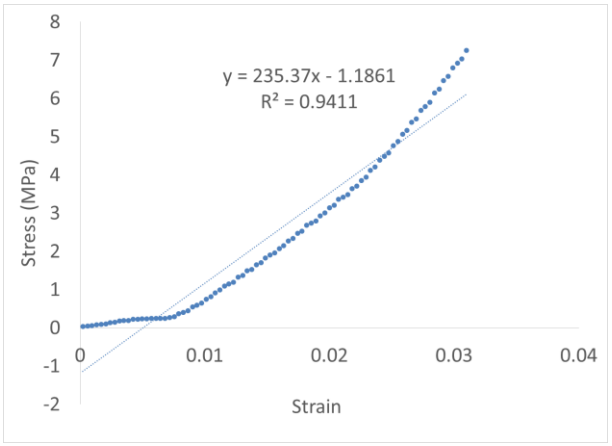

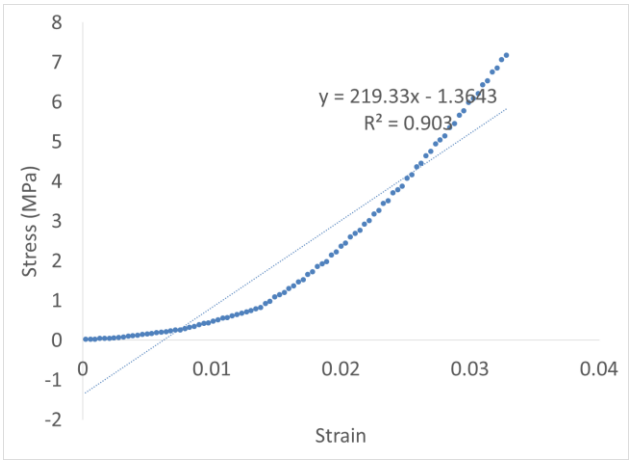

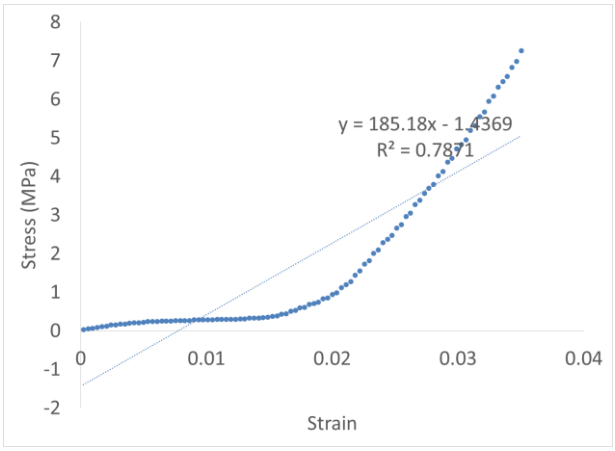

Mechanical experimental data for the compression test of the specimens are tabulated below in table 5. Also the mean young's modulus and the standard deviation are shown in the table.

S.N. / Composition	1	2	3	4	5	6	Mean	SD
5%	239.73	260.91	258.31	281.66	289.43	289.29	269.88	18.35
6%	292.20	301.31	305.94	310.10	290.88	309.93	301.73	7.78
7.5%	326.3	324.38	323.39	321.48	315.91	329.66	323.52	4.24
9%	351.99	237.63	353.73	359.57	348.17	341.97	332.17	42.62
10%	416.87	377.52	364.07	367.15	399.05	376.10	383.46	18.66
12%	447.68	419.30	432.81	432.62	416.87	400.55	424.97	14.88
15%	311.26	313.08	315.91	316.98	321.37	311.82	315.07	3.49
17%	190.16	170.54	235.37	165.70	219.33	185.18	228.10	25.15

Table 5: Modulus of elasticity of each samples, their mean and the standard deviation

It can be seen from the results of the compression test that the young's modulus of each samples are very lower than the actual value, however, a consistency in the increase of the young's modulus are obtained as we go on increasing the glass fiber in the ABS pallets. For 5% GF ABS the average young's modulus is 239.73 MPa and it increases with a factor of 1.1 up to 12% GF ABS which has young's modulus of 424.97 MPa. However, the young's modulus for 15% and 17% GF ABS is not following the pattern which has a very simple explanation. Since we are not able to extrude the filaments by mixing the LLDPE because even a slightest amount of LLDPE on the mixture of

glass fiber and ABS created a problem of coating in the outer surface of the filament, the 3D printer wasn’t able to extrude it through its nozzle. Each time the filament is pushed through the nozzle of the 3D printer the very soft and ductile outer coating of the LLDPE would erode hence decreasing the filament's diameter and the material would clog in the nozzle. As we didn't use the LLDPE, which is supposed to provide some flexibility and ductility in the composition, we used just ABS and GF ABS. So as the percentage of GF increases the filaments become very hard but brittle and the samples printed from such high percentage of GF ABS showed some uneven surfaces and even discontinued layers. This caused several pores inside the sample which while performing the compression test would easily deform and the young's modulus decreased without following the pattern. Likewise, beyond 17% composition of GF ABS, it wasn't possible to extrude the filaments through the nozzle of the 3D printer we had in the lab as the glass fiber would clog in the nozzle and erode it, so we decided to limit our experiment to 17% composition of GF ABS.

Figure 24: Clogged extruder nozzle while extruding higher composition of GF ABS

The young's modulus of the samples after the compression test are still lower than the theoretical values and there are several factors like nozzle temperature, extrusion method, cleanliness of the filament, cooling time of samples, and method and apparatus of the compression test which caused the deviation in the young's modulus. For a simple factor of 5 considering all the experimental variations we would reach the desired value of young's modulus of the samples. The following table shows the mean young's modulus of the samples after multiplying by a factor of 5.

% Composition	5%	6%	7.5%	9%	10%	12%	15%	17%
Mean E (MPa)	1349.44	1508.63	1617.60	1660.88	1917.30	2124.86	1575.35	971.90
Mean E (GPa)	1.345	1.509	1.617	1.661	1.917	2.125	1.575	0.972

Table 6: Mean value of modulus of elasticity considering a factor of 5

For a composition of 10% and 12%, the mechanical properties of the trabecular bone is more justified and hence we have printed the gyroid network for that composition. Printing gyroid are trickier than printing a regular solid prototypes. Gyroid networks have enough hollow spaces within and are connected by curved struts. While 3D printing such objects we face the problems of breakage, uneven surfaces, dislocation from the heated bed, shifted layers, overhangs, weak infills etc. We started printing the gyroids with filaments of PLA and pure ABS which would give us fine prototypes. However, as we print models from composites we had to face above mentioned problems and tackle each problems with some unique solutions. We printed oversized gyroids which were easier to print and go on decreasing its dimensions taking notes of changes in the settings of the slicer software and the modifications in the 3D printer.

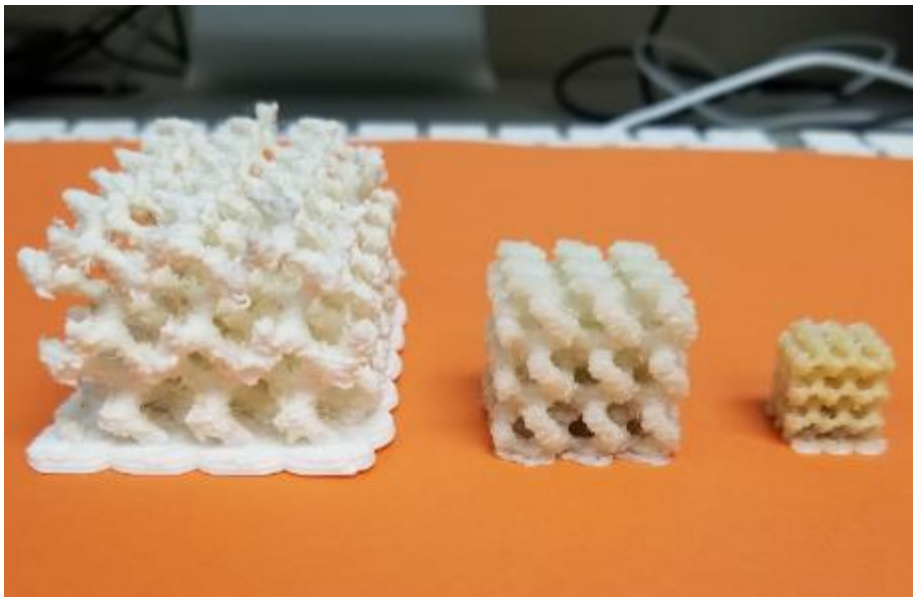

*Figure 25: Gradual decrease in the dimension of the gyroid a) 40*30*30 mm b) 20*20*20 mm c) 15*15*15 mm*

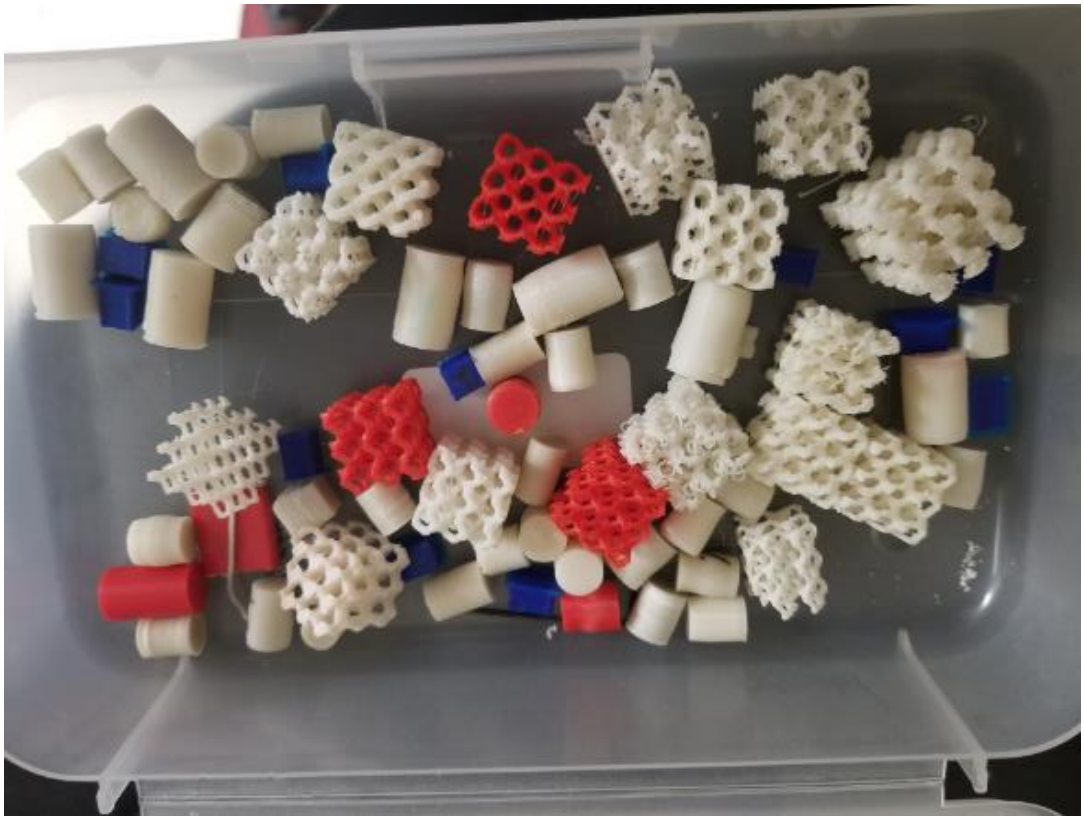

Figure 26: Various samples of different geometry printed before printing a usable test sample

We had to print hundreds of gyroid samples before finally printing the perfect samples which can be used for our test.

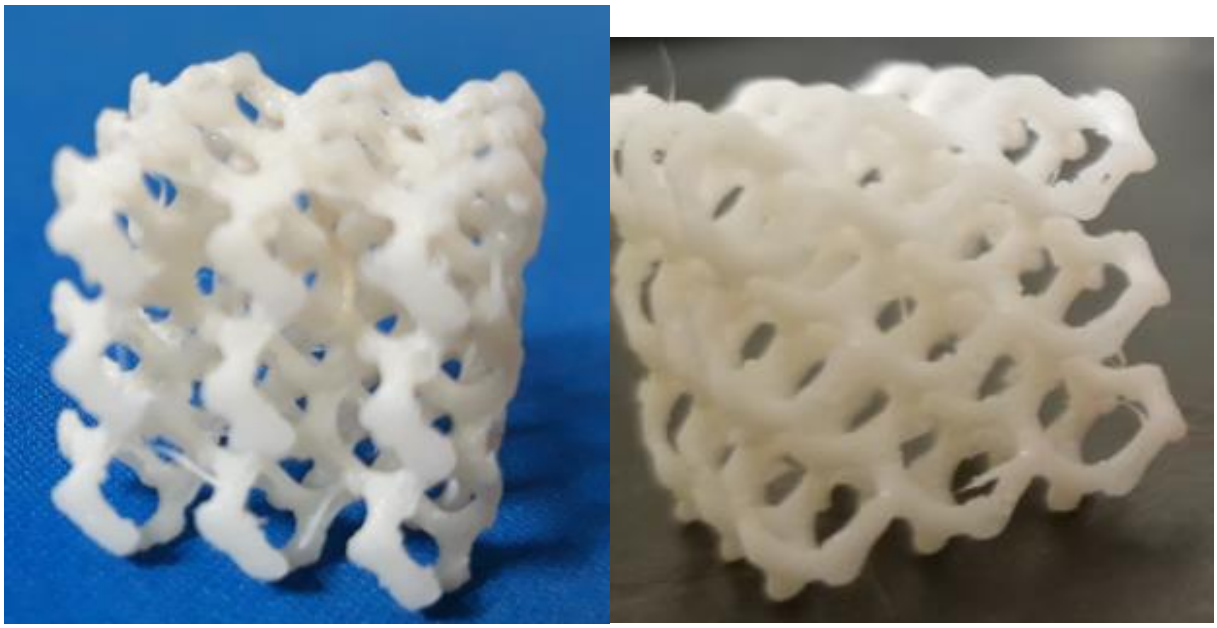

Figure 27: 3D printed gyroids used for compression test

The results of compression test of the gyroid model are presented in the table below. Here also we have assumed a variation by a factor of 5 and hence multiplied each obtained result by 5.

S. N.	1	2	3	4	5	6	Mean E	SD
E (MPa)	388.82	415.25	370.62	391.83	393.41	378.36	389.72	13.93
Mean E after correction factor (MPa)	1944.10	2076.25	1853.10	1959.15	1967.05	1893.61	1948.57	

Table 7: Values of modulus of elasticity of the gyroid obtained from the compression test, its mean and the standard deviation

Plot of stress against strain for gyroid network of six samples.

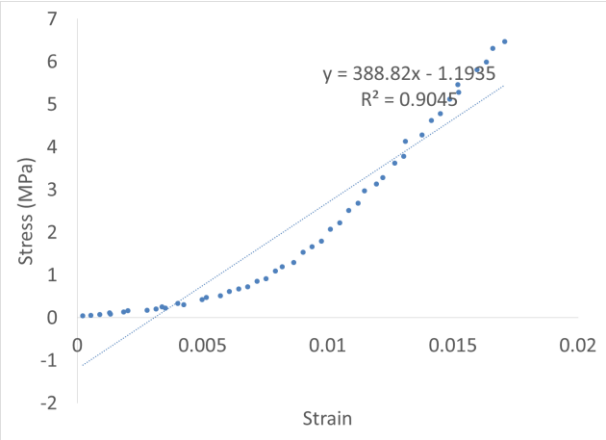

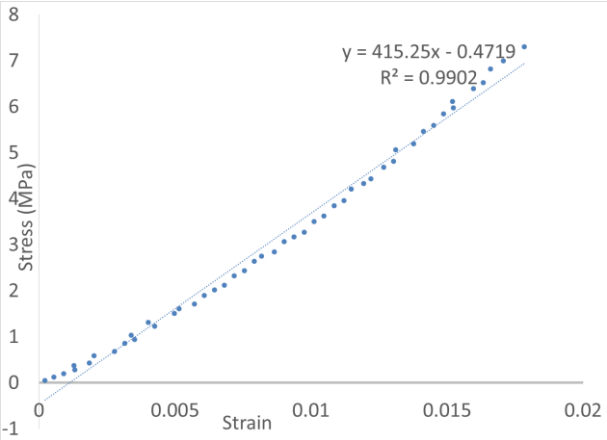

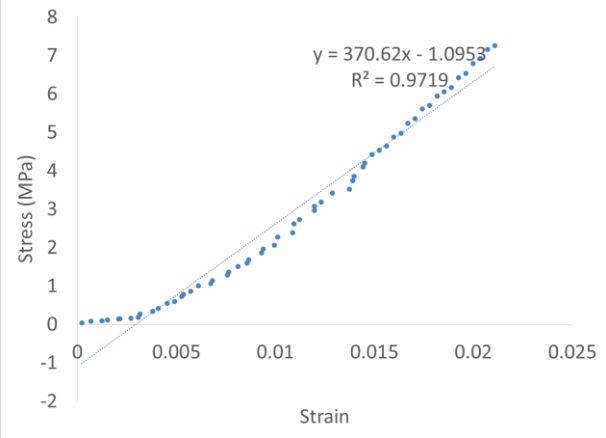

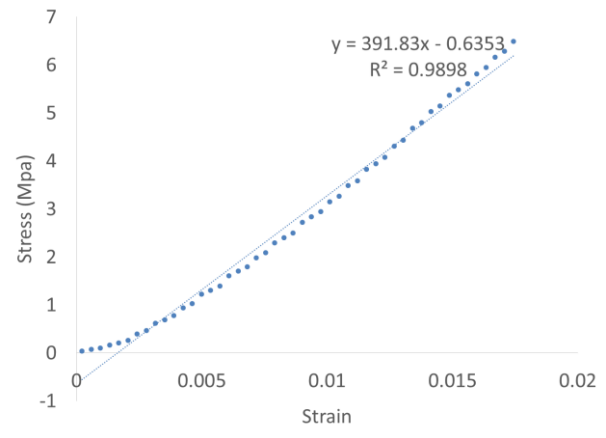

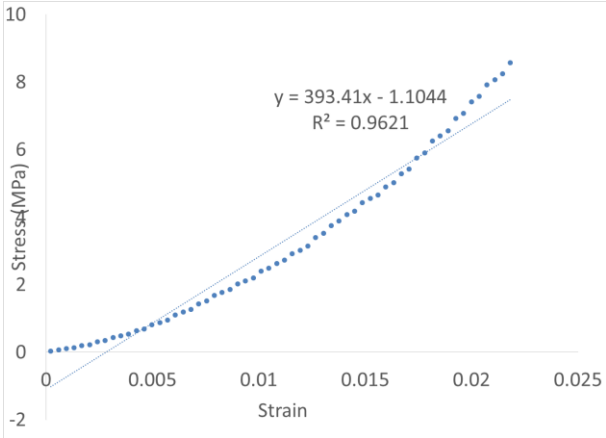

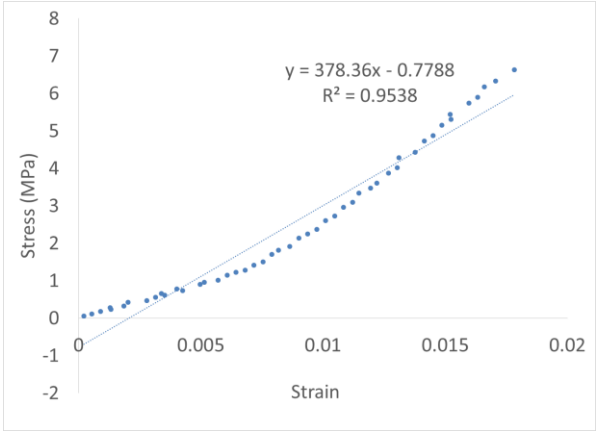

Verification : Apparent density (ρ_{app}) is the wet mineralized mass of the bone at tissue level over the volume occupied by the tissue while the real or material density (ρ_{tis}) is the same mass of the bone material over the total volume occupied by that material. Apparent density is one of the main characteristics of bone which has an influence on the mechanical properties and can influence the compressive properties of bone at tissue level and the material density influence the properties in trabecular level. The modulus of elasticity increases as a higher power or shows exponential relation with the value of apparent density. (Zioupos, Cook, & Hutchinson, 2008)

The following table shows the necessary calculation of apparent density (ρ_{app}) and apparent modulus (E_{app}) and a plot of these two to show the exponential relation between the two.

S.N.	Volume fraction (Vf)	Tissue density (ρ tissue)	App Density (ρ app)	App modulus (E app)	E app (Mpa)
1	0	1.8	0	0	0
2	3	1.8	0.054	0.004421092	4.421092
3	6	1.8	0.108	0.019622037	19.62204
4	9	1.8	0.162	0.046918087	46.91809
5	12	1.8	0.216	0.087088053	87.08805
6	15	1.8	0.27	0.140706808	140.7068
7	18	1.8	0.324	0.208235509	208.2355
8	21	1.8	0.378	0.290061699	290.0617
9	24	1.8	0.432	0.38652098	386.521
10	25	1.8	0.45	0.421978109	421.9781
11	27	1.8	0.486	0.497910169	497.9102
12	30	1.8	0.54	0.624495913	624.4959
13	33	1.8	0.594	0.766520675	766.5207
14	36	1.8	0.648	0.924207055	924.2071
15	39	1.8	0.702	1.097761026	1097.761
16	42	1.8	0.756	1.287374425	1287.374
17	45	1.8	0.81	1.493226908	1493.227

Table 8: Necessary calculation for apparent density and apparent modulus for varying volume fraction

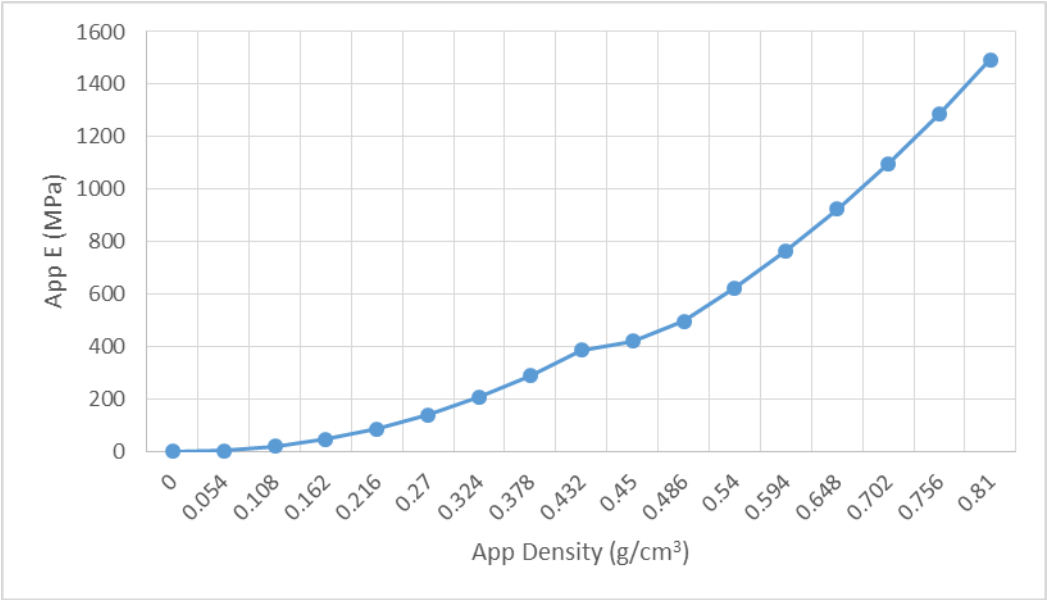

Figure 28: Plot of apparent density and apparent modulus showing the exponential relation

The density of 12% GF ABS is approximately 1.1-1.2 g/cm^3 and for this research purpose if we consider the density to be 1.15 g/cm^3 it gives us an apparent density of 0.2875 g/cm^3 and the calculated apparent modulus is around 161 MPa. From the graph of compression test we have a mean young's modulus of 1948 MPa for a gyroid. As in the literatures cited in section 2.4 we have obtained E_{tissue}= 1948 MPa and since E_{post} =5% E_{tissue} we will have E_{post}= 97 MPa. However, our apparent modulus is around 8% of E_{tissue}.

CHAPTER 5

CONCLUSION AND FUTURE WORKS

5.1 Conclusion

Human trabecular bone has a diverse range of shapes, size, density and mechanical properties depending on the age, health and conditions like osteoporosis. Loss of teeth because of various factors is often common and a replacement of teeth has been carried out for long time. Osseointegrated dental implants are one of the advancement in replacement of teeth.

With several objectives in this research paper we intended to develop a mechanism for selection of screw type dental implants for osteoporotic bones. For this, we first developed a realistic CAD model of trabecular bone. By introducing the parameters like volume fraction, trabecular spacing, trabecular thickness and structural model index we created gyroid to act as a morphological model of trabecular bone.

Subsequently, we synthesize filament composites using ABS and Glass fiber which were used to develop gyroid model so that experimental verification of the mechanical properties can be carried out. By using 12% GF ABS we were able to reach the nearest value of young's modulus of trabecular jaw bone though there is no such experiment which would give us a definite value. We took this composition for the purpose of our research since the samples showed consistency while printing and the modulus value was also high enough to represent actual trabecular bone property. However, we couldn't verify the bilinear elastic-plastic nature of trabecular bone since obtaining a graph in the post modulus region would require a very high initial load. However, simple mathematical calculation would give us a post modulus around 8% of the pre modulus, but the authenticity of this type of experiment is a doubt.

We also derived few mathematical relations for the development of screw-type implant and studied various features and parameters that affect the stability of an implant. However, development of a realistic CAD model is left for a possible future work.

This research uses composite materials to print the gyroid models so that we can develop trabecular bones with volume fraction from 5% to almost 65%. However, samples from fresh jaw bone cadaver can give the best result to find the modulus of the trabecular jaw bone. One of the drawback while using the cadaver is difficulty to prepare the sample to meet the test requirements and the time frame and extended work to determine the volume fraction of each samples through CT scanning. Technically it is very difficult and rare to find cadaver of trabecular jawbone with varying volume fraction or density, so we would be doing the analysis on only a specific volume fraction of trabecular jawbone. Our test will be limited to few number of samples and hence we might not be able to develop the mechanism to determine the best implant for patient specific jaw bone. But again it's hard to establish a clinical feasibility or possibility by performing the test on the composite materials.

5.2 Future work

This research has a very wide objective of selecting a definite type of implant for people with varying property of trabecular jaw bone. As initially targeted, but couldn't be carried out, there are still several sub-tasks that needs to be carried out.

Compression test needs to be done applying large enough force to obtain a curve at post elastic region which can be used to justify the bilinear elastic-plastic region with the predetermined 5% variation.

Finite element analysis of the gyroid network need to be performed to verify the compression test result. However, it should be noted that while selecting the material properties in ANSYS we must determine some basic mechanical properties of the composite nature of GF ABS.

Further, screw-type implants with necessary geometrical features can be produced and tests like pull-out test can be performed to see the force that an implant can withstand without distorting the biomechanical ability.

References

1. *3D Printing*. (2019, 10 21). Retrieved from https://3dprinting.com/pricewatch/3d-printer/qidi-tech-x-max/

2. Aaitmoussa, A., & Yadav, R. (2017). Optimization of a Functionally Graded Material Stem in the Femoral Component of a Cemented Hip Arthroplasty: Influence of Dimensionality of FGM. *Journal of Medical Engineering*.

3. Abhishek, V. R. (2014). *Development and Application of a Morphological Model for Trabecular Bone*. National University of Singapore.

4. Agarwal, V. (2018, 11 05). Retrieved from getreferralmd: https://getreferralmd.com/2018/11/factors-impacting-dental-implants-market-growth/

5. Aitmoussa, A., Yadav, R., Fisher, J., & Khandaker, M. (2017). Minimizing Stress Shielding and Cement Damage in Cemented Femoral Component of a Hip Prosthesis through Computational Design Optimization. *Advances in Orthopedics*.

6. American Society for Testing and Materials. (2009). *Standard Specification for Rigid Poluurethane Foam for Use as a Standard Material for Testing Orthopaedic Deices and Instruments.* ASTM.

7. Bayraktar, H., Morgan, E., Niebur, G., Morris, G., Wong, E., & Keaveny, T. (2004). Comparison of the Elastic and Yield Properties of Human Femoral Trabecular and Cortical Bone Tissue. *Journal of Biomechanics*, 27-35.

8. Bouxsein, M. L., Boyd, S. K., Christiansen, B. A., Guldberg, R. E., Jepsen, K. J., & Muller, R. (2010). Guideline for Assessment of Bone Microstructure in Rodents using Micro-Computed Tomography. *Journal of Bone and Mineral Research, 25*(7).

9. Branemark, P., Hansson, B., Adell, R., Breine, U., Lindstrom, J., Hallen, O., & Ohman, A. (1977). Osseointegrated Implants in the Treatment of the Edentolous Jaw. Experience from a 10-Year Period. *Scandinavian Journal of Plastic and Reconstructive Surgery*.

10. Brunski, J. (1988). Bionaterials and Biomechanics in Dental Implant Design. *International Journal of Oral Maxillofollic Surgery, 3*, 85-97.

11. Carter, D., & Hayes, W. (1977). The Compressive Behaviour of Bone as a Two-Phase Porous Structure. *The Journal of Bone and Joint Surgery*, 954-962.

12. Copper, L. (2000). A Role of Surface Topography in Creating and Maintaining Bone at Titanium Endosseous Implants. *Journal of Prosthetic Dentistry, 84*, 522-534.

13. Davies, J. E. (2003). Understanding Peri-Implant Endosseous Healing. *Journal of Dental Education, 67*.

14. Day, J., Ding, M., Odgaard, A., Sumner, D., Hvid, I., & Weinans, H. (2000). Parallel Plate Model for Trabecular Bone Exhibits Volume Fraction-Dependent Bias. *Bone*, 715-720.

15. Doland, B., Dwight, D., & Tony, K. (2006). *Orthopaedic Biomechancis: Mechanics and Design in Musculoskeletal Systems.* Prentice Hall.

16. Dows Institute of Dental Research. (1999). Biomechanical and Functional Behavior of Implants. *Advances in Dental Research, 13*, 88-92.

17. Drysdale, C., Feran, P., Henderson, S., Parker, C., Speechley, D., Ucer, C., . . . Slade, K. (2012). A Dentist's Guide to Implantology. In A. o. implantology.

18. Dunlop, J., Chong, A., Lucas, G., & Cook, F. (2008). Structural Properties of a Novel Design of Composite Analogue Humeri Models. *Ann Biomed Eng, 36*.

19. Elfar, J., & Stanbury, S. (2014). Composite Bone Models in Orthopaedic Surgery Research and Education. *Journal of Americal Academy of Orthopaedic Surgeons, 22*, 111-120.

20. Friberg, B., Jemt, T., & U, L. (1991). Early Failures in 4641 Consecutively Placed Branemark Dental Inplant: A Study from Stage 1 surgery to the Connection of Completed Prosthesis. *International Journal of Oral Maxillofollic Surgery, 6*, 142-146.

21. Gaviria, L., Salcido, J., Guda, T., & Ong, J. (2014). Current Trends in Dental Implants. *Journal of The Korean Association of Oral and Maxillofacial Surgeons*.

22. Gaviria, L., Salcido, J., Guda, T., & Ong, J. (2014). Current Trends in Dental Implants. *Journal of the Korean Association of Oral and Maxillofacial Surgeons, 40*, 50-60.

23. Geng, J., Ma, Q., Xu, W., Tan, K., & Liu, G. (2004). Finite Element Analysis of Four Thread-Form Configuration in a Stepped Screw Implant. *Journal of Oral Rehabilitation*.

24. Gibson, L., & Ashby, M. (1999). *Cellular Solids, Structure and Properties.* Cambridge University Press.

25. Glauser, R., Ree, A., Lundgren, A., Gottlow, J., Hammerle, C., & Scharer, P. (2003). Immediate Occlusal Loading of Branemark Ti Unite Implants Placed Predominantly in Soft Bone: 1 Year Results of Prospective Clinical Study. *Clinical Inplant Dentistry and Clinical Research, 5*, 47-56.

26. Haas, R., Bernhart, T., Ortbudak, D., & Mailath, G. (1999). Experimental Study of the Damping Behaviour of imz Implants. *Journal of Oral Rehabilitation, 26*, 19-24.

27. Hart, N., Nimphius, S., Rantalainen, T., Ireland, A., Siafarikas, A., & Newton, R. U. (2017). Mechanical Basis of Bone Strength: Influence of Bone Material, Bone Structure and Muscle Action. *Journal of Musculoskeletal and Neuronal Interactions, 17*(3), 114-139.

28. Heller, A., & Heller, R. (1996). Clinical Evolutions of a Porous-Surfaced Endosseous Implant System. *Journal of Oral Implantology, 22*, 240-246.

29. Hildebrand, T., & Ruegsegger, P. (1997). Quantification of Bone Microarchitecture with the Structure Model Index. *Computer Methods in Biomechanics and Bio Medical Engineering*, 15-23.

30. Hill, R. (1952). The Elastic Behavior of a Crystalline Aggregate. *Proceedings of the Physical Society*, 349.

31. Jung, TH, Jay, W., Heng, H., Michael, C., Lih, J., & Jui, T. (2013). Trabecular Bone Structure Parameters Evaluated Using Dental Cone-Beam Computed Tomography: Cellular Synthetic Bones. *BioMedical Engineering Online, 12*.

32. Keller, T. (1994). Predicting the Compressive Mechanical Behavior of Bone. *Journal of Biomechcics*, 1159-1168.

33. Kim, J., Baek, S., Kim, T., & Chang, Y. (2008). Comparison of Stability Between Cylindrical and Conical Type Mini- Implants. Mechancial and Histological Properties. *The Angle Orthodonist*.

34. Kohn, D., Ko, C., & Hollister, S. (1992). Localized Stress Analysis of Dental Implants using Homogenization Theory. *ASME-BED Advances in Bioengineering Winter Annual Meeting of the American Society of Mechanical Engineers. 22*, pp. 607-610. New York: ASME.

35. Lakatos, E., Magyar, L., & Bojtar, I. (2014). Material Properties of the Mandibular Trabecular Bone. *Journal of Medical Engineering, 2014*.

36. Lee, B., Abdullah, J., & Khan, Z. (2005). OPtimization of Rapid Prototyping Parameters for Production of Flexible ABS Object. *Journal of Materials Processing Technology, 169*, 54-61.

37. Lin, D., Li, Q., Li, W., & Swan, M. (2009). Dental Implant Induced Bone remodelling and Associated Algorithms. *Journal of the Mechanical Behavior of Biomedical Materials, 2*, 410-432.

38. Maria, F. V., Helena, C., & Joao, E. F. (2011). Bone: A Composite Natural Material. In *Advances in Composite Materials-Analysis of Natural and Man-Made Materials* (pp. 195-220).

39. Mathieu, V., Vayron, R., Richard, G., Lambert, G., Naili, S., meninngaud, j., & Haiat, G. (2014). Biomechancal Determinants of the Stability of Dental Implants: Influence of the Bone-Implant Interface Properties. *Journal of Biomechanics, 47*, 1. Retrieved from www.elsevier.com/locate/jbiomech

40. MatWeb LLC. (2019, 11 1). *MatWeb: Material Property Data*. Retrieved from http://www.matweb.com/search/datasheet.aspx?matguid=eb7a78f5948d481c9493a67f0d089646&n=1

41. Muller, R., Campenhout, H. V., Damme, B. V., Perre, V., Dequeker, J., Hildebrand, T., & Ruegsegger, P. (1998). Morphometric Analysis of Human Bone Biopsies: A Quantative Structural Comparison of Histological Sections and Micro-Computed Tomography. *Bone*, 59-66.

42. Ogawa, T., Possemiers, T., Zhang, X., Naert, I., Chaudhari, A., Sasaki, K., & Duyck, J. (2011). Influence of Whole Body Vibration Time on Peri-Implant Bone Healing: A Histomorphometrical Animal Study. *Journal of Clinical Periodontology*, 601-609.

43. *Ohaus Corporation*. (2019, 10 21). Retrieved from https://us.ohaus.com/en-US/TripleBeam700Series

44. O'Mahony, A., Williams, J., & Spencer, P. (2001). Anisotropic Elasticity of Cortical and Cancellous Bone in the Posterior Mandible Increase Peri-Implant Stress and Strain under Oblique Loading. *Clinical Oral Implants Research*, 648-657.

45. Patel, S., Shepherd, E., & Hukins, W. (2008). Compressive Properties of Commercially Available Polyurethane Foams as Mechanical Models for Osteoporotic Human Cancellous Bone. *BMC Musculoskeletal Disorder, 9*.

46. Phil, L., Ohlsson, C., & Michael, D. (2015). Structure Model Index Does Not Measure Rods and Plates in Trabecular Bone. *Front Endocrinol*.

47. Pilliar, R., Lee, J., & Maniatoloulos, C. (n.d.). Observations on the Effect of Movement on Bone Ingrowth into Porous-Surfaced Implants . *Clinical Orthopaedics and Related Research*, 108-113.

48. Rho, J., Hobatho, M., & Ashman, R. (1995). Relations of Mechanicla-Properties to Density and CT Numbers in Human Bone. *Medical Engineering and Physics*, 347-355.

49. Rho, J., Kuhn-Spearing, L., & Zioupos, P. (1998). Mechancial Properties and the Hierarchical Structure of Bone. *Medical Engineering and Physics, 20*, 92-102.

50. Stauber, M., & Muller, R. (2006). Age-related changes in Trabecular Bone Microstructures: Global and Local Morphometry. *Osteoporosis International*, 616-626.

51. Sung, H., Michael, M., Dan, O., Shad, R., & Paul, K. (2002). Anisotropic Material Properties of Fused Deposition Modeling ABS. *Rapid Prototyping, 8*(4), 248-257.

52. Sutpideler, M., Eckert, S., Zobitz, M., & An, K. (2004). Finite Element Analysis of Prosthesis Height, Angle of Force Application and Implant Offset on Supporting Bone. *International Journal of Oral and Maxillofacial Implants*, 819-825.

53. Szivek, J., & Gealer, R. (1991). Technical Note: Comparison of the Deformation Response of Synthetic and Cadeveric Femora. *Journal of Applied Biomaterials, 2*, 227-280.

54. Szmukler, S., Y, R., & Dubruille, J. (1998). Timing of Loading and Effect of Micromotion on Bone-Dental Implant Interface. *Journal Of Biomedical Material Research, 43*, 192-203.

55. Vidyasagar, L., & Apse, P. (2004). Dental Implant Design and Biologial Effects on Bone-Implant Interface. *Baltic Dental and Maxillofacial Journal, 6*, 51-54.

56. *Wellzoom Desktop Filament Extruder*. (2019, 10 21). Retrieved from Wellzoom: http://wellzoomextruder.com/product/wellzoom-desktop-filament-extruder-b/

57. Zioupos, P., Cook, R., & Hutchinson, J. (2008). Some Basis Relationships Between Density Values in Cancellous and Cortical Bone. *Journal of Biomechanics, 41*, 1961-1968.

58. Zixiang, W., Jianlei, W., Senthil, T., & Lixin, W. (2016). Mechanical and Thermal Properties of ABS/ Montmorillonite Nanocomposites for Fused Deposition Modeling 3D Printing. *Materials and Design, 102,* 276-283.

59. Zohdi, T., & Wriggers, P. (2008). *An Introduction to Computational Micromechanics* (2nd ed., Vol. 20). Springer.